arXiv:1002.1470v2 [hep-ph] 7 Apr 2010

Polarized pK^- scattering in Unitary Baryon Chiral Perturbation Theory

Antonio O. Bouzas *
Departamento de Física Aplicada, CINVESTAV-IPN
Carretera Antigua a Progreso Km. 6, Apdo. Postal 73 "Cordemex"
Mérida 97310, Yucatán, México

Abstract

We study pK^- scattering in the energy range from threshold through the $\Lambda(1520)$ peak in UBChPT, taking into account $\mathcal{O}(q)$ vertices from meson-baryon contact interactions and s- and u-channel ground-state baryon exchange, s- and u-channel decuplet- and nonet-baryon exchange and t-channel vector-meson exchange, as well as $\mathcal{O}(q^2)$ flavor-breaking vertices. Detailed fits to data are presented, including a substantial body of differential cross-section data with meson momentum $q_{\rm lab} > 300$ MeV not considered in previous treatments.

1 Introduction

The low energy dynamics of hadrons is succesfully described by Chiral Perturbation Theory (ChPT), the effective field theory of meson interactions (see, for example, [1–3] for recent reviews and [4, 5] for textbook expositions). The effective chiral framework can also be extended to the one-baryon sector, where a fully relativistic Baryon Chiral Perturbation Theory (BChPT) has been formulated, describing baryon interactions at low energies (recent reviews are given in [3,6]). The domain of applicability of BChPT is limited to energies near the reaction threshold at which meson momenta are much smaller than the chiral symmetry breaking scale. In the case of $N\overline{K}$ scattering, however, the strong coupling among the different open channels renders the theory inapplicable even at threshold.

Those limitations of BChPT have motivated the introduction of unitarization techniques to extend its phenomenological scope to higher energies in $N\pi$ and NK^+ processes, and to the $S = -1$ sector. Unitary coupled-channels techniques based on Lippmann–Schwinger or Bethe–Salpeter equations have been succesfully applied to the study of $N\overline{K}$ and other meson–baryon processes, even at relatively high energies [7–14]. A unitarization method dealing directly with the chiral effective theory T-matrix was introduced in [15, 16], drawing elements from the N/D method of [17] and from analogous approaches in the meson sector [18, 19]. This Unitary Baryon Chiral Perturbation Theory (UBChPT) has been shown to give good descriptions of cross-section data in $N\overline{K}$ processes [16, 20–22], and in $N\pi$ scattering beyond the Δ resonance peak [15, 23].

In this paper we study pK^- scattering in the energy range from threshold through the $\Lambda(1520)$ peak, corresponding to laboratory-frame incident-meson momentum $0 \leq q_{\rm lab} \lesssim 600$ MeV, in UBChPT. Specifically, with tree-level BChPT partial waves as input for the unitarization approach of [15, 16], we obtain the unitarized partial waves needed to compute physical observables such as total and differential cross sections and spin asymmetries, subsequently fit to experimental data. We take into account in our tree-level amplitudes $\mathcal{O}(q)$ vertices[1] from meson-baryon contact interactions and s- and u-channel ground-state baryon exchange, s- and u-channel decuplet- and nonet-baryon exchange and t-channel vector-meson exchange, as well as $\mathcal{O}(q^2)$ flavor-breaking vertices. We include S, P and D partial waves in our computations, the contribution from F and higher waves being negligibly small at the energies considered here. A global fit to pK^- data over a similar energy range, also including $N\pi$ and pK^+ data, was carried out in [13] in the unitarization framework of the Bethe–Salpeter equation. Unlike [13], however, we explicitly take into account vector-meson exchange, whose contribution is expected to be significant in this context and, as discussed

*E-mail: abouzas@mda.cinvestav.mx

[1] $\mathcal{O}(q^n)$ denotes a generic quantity of chiral order n, with q a nominally small quantity such as a meson momentum or mass.

below, plays a crucial role in the fits to data presented here. Furthermore, we include in our fits a substantial body of differential cross-section data with meson momentum $q_{\rm lab} > 300$ MeV not considered in previous chiral-theoretic treatments.

There is by now overwhelming evidence that the nonets of $J^P = 1/2^-$ and $3/2^-$ baryon resonances [24] are generated by chiral coupled-channels dynamics. The resonance $\Lambda(1405)$ has been shown to be dynamically generated in [10, 13, 16, 21]. Similarly, the resonances $\Lambda(1670)$ and $\Sigma(1620)$ are dynamically generated in UBChPT in [22, 25, 26]. Further examples of the description of nonet baryons as dynamical resonances are $N(1520)$ [26, 27], $N(1535)$ [8, 27, 28], $\Lambda(1520)$ [26]. There is a profuse literature on dynamical generation of resonances in UBChPT that we cannot describe in detail here; recent reviews are given in [29–31]. It should be mentioned that a "static," quark-level component of the $1/2^-$ and $3/2^-$ baryon nonets cannot be ruled out at present. In fact, the existence of such a static component has been advocated, e.g., in [32] in the case of $N(1535)$ and in [33] for $\Lambda(1520)$. In this paper we treat the $3/2^-$ baryon nonet as static, described by an explicit field in the chiral Lagrangian, whereas the $1/2^-$ nonet is dynamically generated. We remark that no global fit to pK^- scattering data including a dynamic $3/2^-$ baryon nonet has been given yet. We consider the present treatment a necessary previous step.

The paper is organized as follows. In sect. 2 we discuss the computation of tree-level amplitudes for baryon–meson scattering in BChPT and their associated partial waves, providing explicit expressions for those amplitudes and partial waves that have not been given in the previous literature. In sect. 3 we briefly discuss the unitarization procedure [15, 16] applied in UBChPT. Our results are presented in sect. 4, where we describe our fitting procedure and best-fit parameters, and detailedly confront computed observables with experimental data. Sect. 5 contains some final remarks. We gather technical material, needed in sect. 2, in the appendices at the end of the paper.

2 Tree-level partial waves

The ground-state meson and baryon octets are described by standard [5] traceless 3×3 complex matrix fields ϕ and B, resp., with ϕ hermitian. We use the physical flavor basis

$$\begin{aligned} \beta^1 &= \frac{1}{\sqrt{2}}\left(\lambda^1 + i\lambda^2\right), \quad \beta^2 = \beta^{1\dagger}\,, \quad \beta^3 = \lambda^3\,, \\ \beta^4 &= \frac{1}{\sqrt{2}}\left(\lambda^4 + i\lambda^5\right), \quad \beta^5 = \beta^{4\dagger}\,, \quad \beta^6 = \frac{1}{\sqrt{2}}\left(\lambda^6 + i\lambda^7\right), \quad \beta^7 = \beta^{6\dagger}\,, \quad \beta^8 = \lambda^8\,, \end{aligned} \tag{1}$$

where λ^a are SU(3) Gell-Mann matrices. The $SU(3)$ algebra in this basis is described in sect. 2 of [23].

Defining the T-matrix as $S = I + i(2\pi)^4\delta(P_f - P_i)T$, the scattering amplitudes are given by T-matrix elements ${\mathcal{T}^{ab}}_{a'b'}(s,u;\sigma,\sigma') \equiv \langle B_{a'}(p',\sigma')M_{b'}(q')|T|B^a(p,\sigma)M^b(q)\rangle$ as functions of the Mandelstam invariants $s = (p+q)^2$, $u = (p-q')^2$ and the spin variables. The center-of-mass frame (CMF) partial waves ${f_{\ell\pm}}^{ab}_{\ a'b'}$ corresponding to $j = \ell \pm 1/2$ are defined as,

$$\begin{aligned} {\mathcal{T}^{ab}}_{a'b'}(s,u;\sigma,\sigma') = \sum_{\ell=0}^{\infty} \Big\{ &\left((\ell+1){f_{\ell+}}^{ab}_{\ a'b'} + \ell {f_{\ell-}}^{ab}_{\ a'b'} \right) P_\ell(\widehat{p}\cdot\widehat{p}')\chi'^{\dagger}_{\sigma'}\cdot\chi_\sigma \\ &+ i\left({f_{\ell+}}^{ab}_{\ a'b'} - {f_{\ell-}}^{ab}_{\ a'b'} \right) P'_\ell(\widehat{p}\cdot\widehat{p}')\chi'^{\dagger}_{\sigma'}\cdot(\vec{\sigma}\cdot(\widehat{p}\wedge\widehat{p}'))\chi_\sigma \Big\}\,, \end{aligned} \tag{2}$$

with $\widehat{p}\cdot\widehat{p}' = \cos\theta_{CM}$, P_ℓ and P'_ℓ the Legendre polynomial of order ℓ and its derivative, and χ_σ, $\chi'_{\sigma'}$ 2-component spinors for the initial and final baryon, resp.

2.1 Partial waves from octet-baryon exchange

The Lagrangian of fully relativistic Baryon Chiral Perturbation Theory (BChPT) is written as a sum $\mathcal{L} = \mathcal{L}_M + \mathcal{L}_{MB}$ of a purely mesonic Lagrangian $\mathcal{L}_M$ and a meson–baryon one $\mathcal{L}_{MB}$. The mesonic Lagrangian to $\mathcal{O}(q^4)$ was first obtained in [34, 35]. The meson–baryon Lagrangian $\mathcal{L}_{MB}$ has been given to $\mathcal{O}(q^3)$ in the three-flavor case in [36] (see also [37–39]), and in [40] for two flavors. The tree-level amplitudes from $\mathcal{L}$ for meson-baryon scattering have been given in [16] (see also [20, 41]). The associated CM-frame partial waves have been given in full detail in [23], so there is no need to repeat them here. We emphasize that the partial

waves of [23], as well as those given below, are valid only within the physical region for the process being considered, away from which appropriate analytic continuation is necessary.

2.2 Partial waves from decuplet-baryon exchange

For decuplet-baryon exchange diagrams at tree level, our starting point is the relativistic Lagrangian for Δ-N-π interaction from [42] (see also, e.g., [43–45]). At leading chiral order the transition from two to three flavors amounts to inserting in the amplitudes the flavor factors for the coupling of two octets and a decuplet. The tree-level scattering amplitudes so obtained differ from those for $N\pi$ scattering [15] only in their flavor coefficients. The CMF partial waves for tree-level s-channel decuplet exchange given in [23] are used here without modification. We discuss here u-channel decuplet-baryon exchange, which was not given explicitly in [23], and below similar results are presented for s- and u-channel nonet-baryon and t-channel vector-meson exchange amplitudes.

The tree-level contribution of u-channel decuplet exchange to the T-matrix can be parameterized as,

$$\mathcal{T}_{(u,\mathrm{dec})}{}^{ab}{}_{a'b'} = \frac{9}{8} g_{10}^2 \frac{(D+F)^2}{f^2} \sum_{C=1}^{10} \frac{\mathcal{S}_{a'}{}^{b}{}_{C} \mathcal{S}^{a}{}_{b'C}}{u - M_C^2 + i0} \overline{u}' \left(\widehat{\Gamma}_{(u,\mathrm{dec})0}{}^{ab}{}_{a'b'C} + \widehat{\Gamma}_{(u,\mathrm{dec})1}{}^{ab}{}_{a'b'C} \not{p}_T \right) u \ , \tag{3}$$

where g_{10} is a coupling constant allowing for departures from the SU(6) symmetric case $g_{10} = 1$, and u and u' are the Dirac spinors for the initial and final baryon. The flavor coefficients attached to each vertex in (3) are given by,

$$\mathcal{S}_{a'}{}^{b}{}_{C} = \frac{1}{2} \varepsilon_{ilm} (\beta^\dagger_{a'})_{lj} (\beta^b)_{mk} (T_C)_{ijk} \ , \quad \mathcal{S}^{a}{}_{b'C} = \frac{1}{2} \varepsilon_{ilm} (\beta^a)_{jl} (\beta^\dagger_{b'})_{km} (T_C)_{ijk} \ , \tag{4}$$

with repeated indices i, j, …, summed from 1 to 3, and the matrices β from (1). T_C in (4) are a standard basis for the decuplet representation space (as given, e.g., in eq. (9) of [46]). In order to fully specify the reduced amplitudes in (3) we expand them as,

$$\widehat{\Gamma}_{(u,\mathrm{dec})0}{}^{ab}{}_{a'b'C} = \widehat{\Gamma}_{(u,\mathrm{dec})0.0}{}^{ab}{}_{a'b'C} + \widehat{\Gamma}_{(u,\mathrm{dec})0.1}{}^{ab}{}_{a'b'C}\, u + \widehat{\Gamma}_{(u,\mathrm{dec})0.2}{}^{ab}{}_{a'b'C}\, u^2 + \widehat{\Gamma}_{(u,\mathrm{dec})0.3}{}^{ab}{}_{a'b'C}\, t \ , \tag{5}$$

with the coefficients on the r.h.s. independent of u and t, and similarly $\widehat{\Gamma}_{(u,\mathrm{dec})1}{}^{ab}{}_{a'b'C}$. This expansion is also needed to compute the partial waves associated to the amplitude (3). Explicit calculation yields,

$$\begin{aligned}
\widehat{\Gamma}_{(u,\mathrm{dec})0.0}{}^{ab}{}_{a'b'C} &= \frac{1}{3}(m_{a'}\widetilde{m}_b^2 + m_a \widetilde{m}_{b'}^2)(1-\kappa) + \frac{1}{6}(m_{a'}^3 + m_a^3)(1+2\kappa) \\
&\quad + \frac{1}{3}(m_a m_{a'}^2 + m_a^2 m_{a'})(1+2\kappa^2) + \frac{1}{2}(m_{a'}\widetilde{m}_{b'}^2 + m_a \widetilde{m}_b^2) \\
&\quad + \frac{M_C}{3}(1-2\kappa+4\kappa^2)(m_{a'}^2 + m_a m_{a'} + m_a^2) + \frac{M_C}{2}(\widetilde{m}_{b'}^2 + \widetilde{m}_b^2) \\
&\quad + \frac{1}{6M_C}\left(\widetilde{m}_{b'}^2 (m_{a'}^2 - \widetilde{m}_b^2) + \widetilde{m}_b^2 (m_a^2 - \widetilde{m}_{b'}^2) + m_{a'} m_a (m_{a'}^2 + m_a^2 - \widetilde{m}_{b'}^2 - \widetilde{m}_b^2) \right) \\
&\quad - \frac{1}{6M_C^2}(m_a + m_{a'})(m_a^2 - \widetilde{m}_{b'}^2)(m_{a'}^2 - \widetilde{m}_{b'}^2) \ , \\
\widehat{\Gamma}_{(u,\mathrm{dec})0.1}{}^{ab}{}_{a'b'C} &= -\frac{1}{6}(m_{a'} + m_a)(1+2\kappa) - \frac{1}{3M_C} m_a m_{a'} (1-2\kappa+4\kappa^2) - \frac{1}{6M_C}(\widetilde{m}_{b'}^2 + \widetilde{m}_b^2) \\
&\quad + \frac{2}{3M_C}(m_{a'}^2 + m_a^2)\kappa(1-2\kappa) - \frac{M_C}{3}(1-2\kappa+4\kappa^2) + \frac{1}{6M_C^2}\Big[\Big(m_{a'}(m_{a'}^2 - \widetilde{m}_b^2) \\
&\quad + \ m_a (m_a^2 - \widetilde{m}_{b'}^2) \Big)(1-2\kappa) + m_a m_{a'}(m_a + m_{a'})(1-4\kappa^2) - (m_{a'}\widetilde{m}_{b'}^2 + m_a \widetilde{m}_b^2) \Big] \ , \\
\widehat{\Gamma}_{(u,\mathrm{dec})0.2}{}^{ab}{}_{a'b'C} &= -\frac{2}{3M_C}\kappa(1-2\kappa) - \frac{1}{6M_C^2}(1-2\kappa)(m_a + m_{a'}) \ , \\
\widehat{\Gamma}_{(u,\mathrm{dec})0.3}{}^{ab}{}_{a'b'C} &= -\frac{1}{2}(m_a + m_{a'} + M_C) \ ,
\end{aligned} \tag{6a}$$

and

$$
\begin{aligned}
\widehat{\Gamma}_{(u,\mathrm{dec})1.0}{}^{ab}{}_{a'b'C} &= -\frac{1}{3}(\widetilde{m}_b^2+\widetilde{m}_{b'}^2)(1-\kappa)-\frac{1}{6}(m_{a'}^2+m_a^2)(1+2\kappa)-\frac{1}{3}m_a m_{a'}(1+2\kappa^2)\\
&\quad -\frac{M_C}{3}(m_{a'}+m_a)(1-2\kappa+4\kappa^2)+\frac{1}{6M_C}(\widetilde{m}_{b'}^2 m_{a'}+\widetilde{m}_b^2 m_a-m_a m_{a'}^2-m_a^2 m_{a'})\\
&\quad +\frac{1}{6M_C^2}(\widetilde{m}_b^2\widetilde{m}_{b'}^2-\widetilde{m}_{b'}^2 m_{a'}^2-\widetilde{m}_b^2 m_a^2+m_a^2 m_{a'}^2)\ ,\\
\widehat{\Gamma}_{(u,\mathrm{dec})1.1}{}^{ab}{}_{a'b'C} &= \frac{2}{3}\kappa(1-\kappa)+\frac{1}{6M_C}(m_a+m_{a'})(1-4\kappa+8\kappa^2)\\
&\quad +\frac{1}{6M_C^2}\left[(\widetilde{m}_b^2+\widetilde{m}_{b'}^2-m_a^2-m_{a'}^2)(1-2\kappa)+m_a m_{a'}4\kappa^2\right]\ ,\\
\widehat{\Gamma}_{(u,\mathrm{dec})1.2}{}^{ab}{}_{a'b'C} &= \frac{1}{6M_C^2}(1-2\kappa)^2\ ,\\
\widehat{\Gamma}_{(u,\mathrm{dec})1.3}{}^{ab}{}_{a'b'C} &= \frac{1}{2}\ .
\end{aligned}
\tag{6b}
$$

In this equation $\kappa = Z+1/2$, with Z the off-shell parameter entering the Lagrangian for the Rarita–Schwinger decuplet field.[2] With these coefficients the amplitude (3) is completely specified. From (3) it is immediate that partial waves for u-channel decuplet exchange take the form

$$
f_{(u,\mathrm{dec})\ell\pm}{}^{ab}{}_{a'b'} = \frac{9}{8}g_{10}^2\frac{(D+F)^2}{f^2}\sum_{C=1}^{10}\mathcal{S}_{a'}{}^{b}{}_{C}\,\mathcal{S}^{a}{}_{b'C}\widehat{f}_{(u,\mathrm{dec})\ell\pm}{}^{ab}{}_{a'b'C}\ . \tag{7}
$$

In order to express the reduced partial waves $\widehat{f}_{(u,\mathrm{dec})\ell\pm}{}^{ab}{}_{a'b'}$ in terms of the coefficients (6a), (6b), we need to introduce some further notation. We define,

$$
\widehat{\Gamma}_{(u,\mathrm{dec})\pm.i}{}^{ab}{}_{a'b'C} = \widehat{\Gamma}_{(u,\mathrm{dec})0.i}{}^{ab}{}_{a'b'C} \pm \sqrt{s}\,\widehat{\Gamma}_{(u,\mathrm{dec})1.i}{}^{ab}{}_{a'b'C}\ , \qquad i=0,\ldots,3\ , \tag{8}
$$

and

$$
\mathcal{N} = \sqrt{p^0+m_a}\sqrt{p'^0+m_{a'}}\Big|_{CMF} = \frac{1}{2\sqrt{s}}\sqrt{(\sqrt{s}-m_a)^2-\widetilde{m}_b^2}\sqrt{(\sqrt{s}-m_{a'})^2-\widetilde{m}_{b'}^2}\ . \tag{9}
$$

Notice that $\mathcal{N}$ depends on flavor indices through baryon and meson masses. Its dependence, like that of $\langle u\rangle$ and Δu defined in appendix A, is not made explicit in the notation . The reduced partial waves of (7) are then, omitting flavor indices for simplicity,

$$
\widehat{f}_{(u,\mathrm{dec})\ell+} = H_\ell - \frac{1}{\ell+1}K_\ell\ , \qquad \widehat{f}_{(u,\mathrm{dec})\ell-} = H_\ell + \frac{1}{\ell}K_\ell\ , \tag{10a}
$$

with

$$
H_\ell = \mathcal{N}\sum_{i=0}^{3}\widehat{\Gamma}_{(u,\mathrm{dec})+.i}h_{+.i}^{(\ell)} - \frac{\Delta u}{\mathcal{N}}\sum_{i=0}^{3}\widehat{\Gamma}_{(u,\mathrm{dec})-.i}h_{-.i}^{(\ell)}\ , \qquad K_\ell = -\frac{\Delta u}{\mathcal{N}}\sum_{i=0}^{3}\widehat{\Gamma}_{(u,\mathrm{dec})-.i}k_{-.i}^{(\ell)}\ . \tag{10b}
$$

The integrals $h_{\pm.i}^{(\ell)}$, $k_{-.i}^{(\ell)}$, which like $\widehat{\Gamma}_{(u,\mathrm{dec})\pm.i}$ depend on a, b, a', b', C, are defined in appendix B.

2.3 Partial waves from nonet-baryon exchange

We consider the exchange of nonet baryon resonances with $J^P = 3/2^-$, whose mostly-singlet member $\Lambda(1520)$ features prominently in pK^- scattering cross sections. We describe these resonances as a nonet of Rarita-Schwinger fields, $\mathcal{N}_0$, $\mathcal{N} = 1/\sqrt{2}\sum_{a=1}^{8}\mathcal{N}_a\beta^a$, with the same flavor-matrix representation for $\mathcal{N}$ as for the ground-state baryon octet [23]. These fields are taken to be mass eigenstates, with $\mathcal{N}_0 = \Lambda(1520)$, $\mathcal{N}_{1,2,3} = \Sigma(1620)^{+,-,0}$, $\mathcal{N}_{4,6} = N(1520)^{+,0}$, $\mathcal{N}_{5,7} = \Xi(1820)^{-,0}$, $\mathcal{N}_8 = \Lambda(1690)$. Thus, their interaction

[2]The parameter Z has been shown to be redundant in [47]. A formulation without off-shell parameter is given, e.g., in [45]. We retain the formulation with an off-shell parameter here, to make use of the results of [15, 16, 23].

Lagrangian must take into account the mixing of singlet and octet components of $\mathcal{N}_{0,8}$, but their tree-level propagator is diagonal. For each $\mathcal{N}_a$, its free propagator has the same form as for each member of the decuplet (see, e.g., eq. (3.8) of [15]).

The interaction vertices for nonet and octet baryons and pseudoscalar mesons are described by a Lagrangian with the same Lorentz structure as the Lagrangian for decuplet baryons (except for an additional γ_5 due to the opposite intrinsic parity of nonet and decuplet), and with the same flavor structure as the Lagrangian for ground-state baryons and mesons, augmented by $\mathcal{N}_0$–$\mathcal{N}_8$ mixing. Explicitly

$$\begin{aligned}
f\mathcal{L}_{\rm nnt} &= \sum_{h=1}^{7} \mathcal{F}_{(8)}{}^{c}{}_{d}{}^{h} \partial^\mu \phi_c \overline{B}^d (g_{\mu\nu} - \kappa_9 \gamma_\mu \gamma_\nu) \gamma_5 \mathcal{N}_h^\nu + \cos\theta \mathcal{F}_{(8)}{}^{c}{}_{d}{}^{8} \partial^\mu \phi_c \overline{B}^d (g_{\mu\nu} - \kappa_9 \gamma_\mu \gamma_\nu) \gamma_5 \mathcal{N}_8^\nu \\
&\quad + \sin\theta \mathcal{F}_{(8)}{}^{c}{}_{d}{}^{8} \partial^\mu \phi_c \overline{B}^d (g_{\mu\nu} - \kappa_9 \gamma_\mu \gamma_\nu) \gamma_5 \mathcal{N}_0^\nu + \cos\theta D_0 {\rm Tr}(\partial^\mu \phi_c \overline{B}^d)(g_{\mu\nu} - \kappa_9 \gamma_\mu \gamma_\nu) \gamma_5 \mathcal{N}_0^\nu \\
&\quad - \sin\theta D_0 {\rm Tr}(\partial^\mu \phi_c \overline{B}^d)(g_{\mu\nu} - \kappa_9 \gamma_\mu \gamma_\nu) \gamma_5 \mathcal{N}_8^\nu + {\rm h.c.}\ , \\
\mathcal{F}_{(8)}{}^{c}{}_{d}{}^{h} &\equiv D_8 d^{c}{}_{d}{}^{h} - F_8 f^{c}{}_{d}{}^{h}\ ,
\end{aligned} \tag{11}$$

which establishes the definition of our coupling constants and mixing parameter. In (11) D_0, D_8 and F_8 are the singlet, and the D- and F-type octet, couplings, resp., and θ is the nonet mixing angle. It is also apparent in $\mathcal{L}_{\rm nnt}$ that we are using the same off-shell parameter κ_9 for both singlet and octet fields [13]. While there is to our knowledge no reason why those parameters should be precisely equal, we have found that keeping the singlet and octet parameters independent does not lead to improvements in the description of experimental data. Actually, in our experience, the best fits are obtained by setting them to be equal.

The tree-level amplitudes obtained from (11) can be parameterized as,

$$\begin{aligned}
\mathcal{T}_{\rm nnt}{}^{ab}{}_{a'b'} &= \mathcal{T}_{(s,{\rm nnt})}{}^{ab}{}_{a'b'} + \mathcal{T}_{(u,{\rm nnt})}{}^{ab}{}_{a'b'}\ , \\
\mathcal{T}_{(s,{\rm nnt})}{}^{ab}{}_{a'b'} &= \frac{1}{f^2} \sum_{e=0}^{8} \mathcal{F}_{(s,{\rm nnt})}{}^{abe}{}_{a'b'} \frac{1}{s - M_{9_e}{}^2 + i0} \overline{u}' \left(\widehat{\Gamma}_{(s,{\rm nnt})0}{}^{abe}{}_{a'b'} + \widehat{\Gamma}_{(s,{\rm nnt})1}{}^{abe}{}_{a'b'} \not{p}_T \right) u\ , \\
\mathcal{T}_{(u,{\rm nnt})}{}^{ab}{}_{a'b'} &= \frac{1}{f^2} \sum_{e=0}^{8} \mathcal{F}_{(u,{\rm nnt})}{}^{abe}{}_{a'b'} \frac{1}{u - M_{9_e}{}^2 + i0} \overline{u}' \left(\widehat{\Gamma}_{(u,{\rm nnt})0}{}^{abe}{}_{a'b'} + \widehat{\Gamma}_{(u,{\rm nnt})1}{}^{abe}{}_{a'b'} \not{p}_T \right) u\ .
\end{aligned} \tag{12}$$

The flavor index e in the sum runs through the octet ($e = 1, \ldots, 8$) and singlet ($e = 0$) baryon resonances, with M_{9_e} the mass of the $e^{\rm th}$ nonet member. The flavor coefficients in (12) are,

$$\begin{aligned}
\mathcal{F}_{(s,{\rm nnt})}{}^{abe}{}_{a'b'} &= \left(D_8 d^{e}{}_{b'a'} - F_8 f^{e}{}_{b'a'} \right) \left(D_8 d^{ba}{}_{e} + F_8 f^{ba}{}_{e} \right), \qquad e = 1, \ldots, 7\ , \\
\mathcal{F}_{(s,{\rm nnt})}{}^{ab8}{}_{a'b'} &= \left(\cos\theta \left(D_8 d^{8}{}_{b'a'} - F_8 f^{8}{}_{b'a'} \right) - \sin\theta D_0 e_{b'a'} \right) \left(\cos\theta \left(D_8 d^{ba}{}_{8} + F_8 f^{ba}{}_{8} \right) - \sin\theta D_0 e^{ba} \right), \\
\mathcal{F}_{(s,{\rm nnt})}{}^{ab0}{}_{a'b'} &= \left(\sin\theta \left(D_8 d^{8}{}_{b'a'} - F_8 f^{8}{}_{b'a'} \right) + \cos\theta D_0 e_{b'a'} \right) \left(\sin\theta \left(D_8 d^{ba}{}_{8} + F_8 f^{ba}{}_{8} \right) + \cos\theta D_0 e^{ba} \right), \\
\mathcal{F}_{(u,{\rm nnt})}{}^{abe}{}_{a'b'} &= \left(D_8 d^{be}{}_{a'} + F_8 f^{be}{}_{a'} \right) \left(D_8 d^{ab'}{}_{e} - F_8 f^{ab'}{}_{e} \right), \qquad e = 1, \ldots, 7\ , \\
\mathcal{F}_{(u,{\rm nnt})}{}^{ab8}{}_{a'b'} &= \left(\cos\theta \left(D_8 d^{b8}{}_{a'} + F_8 f^{b8}{}_{a'} \right) - \sin\theta D_0 e^{b}_{a'} \right) \left(\cos\theta \left(D_8 d^{a}{}_{b'8} - F_8 f^{a}{}_{b'8} \right) - \sin\theta D_0 e^{a}_{b'} \right), \\
\mathcal{F}_{(u,{\rm nnt})}{}^{ab0}{}_{a'b'} &= \left(\sin\theta \left(D_8 d^{b8}{}_{a'} + F_8 f^{b8}{}_{a'} \right) + \cos\theta D_0 e^{b}_{a'} \right) \left(\sin\theta \left(D_8 d^{a}{}_{b'8} - F_8 f^{a}{}_{b'8} \right) + \cos\theta D_0 e^{a}_{b'} \right)\ .
\end{aligned} \tag{13}$$

The reduced amplitudes $\widehat{\Gamma}_{(s,{\rm nnt})0,1}$ and $\widehat{\Gamma}_{(u,{\rm nnt})0,1}$ in (12) are obtained from those for the decuplet by substituting $M_C \to -M_{9_e}$ and $\kappa \to \kappa_9$.

From (12) the partial waves for nonet-exchange amplitudes are seen to take the form,

$$\begin{aligned}
f_{(s,{\rm nnt})\ell\pm}{}^{ab}{}_{a'b'} &= \frac{1}{f^2} \sum_{e=0}^{8} \mathcal{F}_{(s,{\rm nnt})}{}^{abe}{}_{a'b'} \frac{1}{s - M_{9_e}{}^2 + i0} \widehat{f}_{(s,{\rm nnt})\ell\pm}{}^{abe}{}_{a'b'}\ , \\
f_{(u,{\rm nnt})\ell\pm}{}^{ab}{}_{a'b'} &= \frac{1}{f^2} \sum_{e=0}^{8} \mathcal{F}_{(u,{\rm nnt})}{}^{abe}{}_{a'b'} \widehat{f}_{(u,{\rm nnt})\ell\pm}{}^{abe}{}_{a'b'}\ .
\end{aligned} \tag{14}$$

In the s-channel case, the partial waves with $j = 3/2$ take a particularly simple form,

$$
\begin{aligned}
f_{(s,\mathrm{nnt})1+}{}^{ab}{}_{a'b'} &= \frac{1}{f^2}\left(-\frac{\mathcal{N}\Delta u}{6}\right)\sum_{e=0}^{8}\mathcal{F}_{(s,\mathrm{nnt})}{}^{abe}{}_{a'b'}\frac{1}{\sqrt{s}+M_{9_e}}\ ,\\
f_{(s,\mathrm{nnt})2-}{}^{ab}{}_{a'b'} &= \frac{1}{f^2}\left(-\frac{\Delta u^2}{12\mathcal{N}}\right)\sum_{e=0}^{8}\mathcal{F}_{(s,\mathrm{nnt})}{}^{abe}{}_{a'b'}\frac{1}{\sqrt{s}-M_{9_e}}\ ,
\end{aligned}
\tag{15}
$$

where $\mathcal{N}$ is defined in (9) and Δu in (A.5). Since, as discussed in section 4, only the $D_{3/2}$ partial wave for nonet exchange enters our analysis, we omit the explicit expressions of the $S_{1/2}$ and $P_{1/2}$ waves for brevity. For the u-channel, the reduced partial waves in (14) can be obtained from those for decuplet-exchange, (10), by means of the substitutions $M_C \to -M_{9_e}$ and $\kappa \to \kappa_9$ in the reduced amplitudes, and the substitution $M_C \to M_{9_e}$ in the integrals $h^{(\ell)}_{\pm.i}$, $k^{(\ell)}_{-.i}$ given in appendix B.

2.4 Partial waves from vector-meson exchange

We expect vector-meson interactions to play a significant role in the energy range $0 \le q_{\mathrm{lab}} \lesssim 600$ MeV considered in this paper. In tree-level chiral perturbation theory, vector mesons contribute to meson–baryon scattering through t-channel exchange. The Lagrangians for pseudoscalar meson–vector meson and ground-state baryon–vector meson interactions have been discussed in [15, 48, 49] and refs. therein. Here we follow the notation of [15]. The coupling constant for the PPV meson vertex is denoted G_V (expressed here in MeV), and there are eight leading-order couplings for baryon–vector meson interactions, denoted $R_{D,F}$, $S_{D,F}$, $T_{D,F}$, $U_{D,F}$, [15] with units $\mathrm{MeV}^{0,-1,-3,-2}$ resp. In the t-channel vector-meson exchange amplitude these couplings appear as products $G_V X_{D,F}$, with $X = R, S, T, U$. The value of $G_V \sim 60$ MeV can be estimated from vector meson decays, or from pseudoscalar-meson electromagnetic form factors [15]. The values of the coupling constants in the three-flavor baryon–vector meson Lagrangian are not well established.

The tree-level t-channel vector-meson exchange contribution to the T matrix can be parameterized as,

$$
\begin{aligned}
\mathcal{T}_{(\mathrm{vec})}{}^{ab}{}_{a'b'} &= \frac{4\sqrt{2}G_V}{f^2}\sum_{X=R,S,T,U}\sum_{c=1}^{8} f^{cb}{}_{b'}\mathcal{X}_c{}^{a}{}_{a'}\frac{1}{t-{M_V}_c^2+i0}\overline{u}'\left(\widehat{\Gamma}_{(X)0}{}^{abc}{}_{a'b'}+\widehat{\Gamma}_{(X)1}{}^{abc}{}_{a'b'}\not{p}_T\right)u\ ,\\
\mathcal{X}_c{}^{a}{}_{a'} &= d_c{}^{a}{}_{a'}X_D + f_c{}^{a}{}_{a'}X_F\ , \qquad X = R, S, T, U\ ,
\end{aligned}
\tag{16}
$$

where $\mathcal{X} = \mathcal{R}, \mathcal{S}, \mathcal{T}, \mathcal{U}$ for $X = R, S, T, U$, resp. We expand the reduced amplitudes in (16) as,

$$
\widehat{\Gamma}_{(X)0}{}^{abc}{}_{a'b'} = \widehat{\Gamma}_{(X)0.0}{}^{abc}{}_{a'b'} + \widehat{\Gamma}_{(X)0.1}{}^{abc}{}_{a'b'}t + \widehat{\Gamma}_{(X)0.2}{}^{abc}{}_{a'b'}t^2 + \widehat{\Gamma}_{(X)0.3}{}^{abc}{}_{a'b'}u\ ,
\tag{17}
$$

and analogously $\widehat{\Gamma}_{(X)1}{}^{abc}{}_{a'b'}$. The coefficients in the r.h.s. of (17) are independent of u and t. Computation at tree level yields the non-vanishing coefficients,

$$
\begin{aligned}
&\widehat{\Gamma}_{(R)0.0}{}^{abc}{}_{a'b'} = -\frac{1}{2}\left(s+(m_a+m_{a'})^2\right)\ ,\quad \widehat{\Gamma}_{(R)0.3}{}^{abc}{}_{a'b'} = \frac{1}{2}\ ,\quad \widehat{\Gamma}_{(R)1.0}{}^{abc}{}_{a'b'} = m_a+m_{a'}\ ,\\
&\widehat{\Gamma}_{(S)0.0}{}^{abc}{}_{a'b'} = \frac{1}{4}(m_{a'}-m_a)(\widetilde{m}_{b'}^2-\widetilde{m}_b^2)\ ,\quad \widehat{\Gamma}_{(S)0.1}{}^{abc}{}_{a'b'} = -\frac{1}{4}(m_a+m_{a'})\ ,\quad \widehat{\Gamma}_{(S)1.1}{}^{abc}{}_{a'b'} = \frac{1}{2}\ ,\\
&\widehat{\Gamma}_{(T)0.0}{}^{abc}{}_{a'b'} = \frac{1}{16}(m_{a'}-m_a)^2(m_a+m_{a'})(2s+2m_{a'}m_a-\widetilde{m}_b^2-\widetilde{m}_{b'}^2)\ ,\\
&\widehat{\Gamma}_{(T)0.1}{}^{abc}{}_{a'b'} = \frac{1}{16}(m_a-m_{a'})(m_a^2-m_{a'}^2+\widetilde{m}_{b'}^2-m_b^2)\ ,\\
&\widehat{\Gamma}_{(T)0.2}{}^{abc}{}_{a'b'} = \frac{1}{16}(m_a+m_{a'})\ ,\quad \widehat{\Gamma}_{(T)1.0}{}^{abc}{}_{a'b'} = -\frac{1}{8}(m_{a'}^2-m_a^2)^2\ ,\quad \widehat{\Gamma}_{(T)1.2}{}^{abc}{}_{a'b'} = -\frac{1}{8}\\
&\widehat{\Gamma}_{(U)0.0}{}^{abc}{}_{a'b'} = \frac{1}{8}(m_a-m_{a'})\left(m_am_{a'}(m_a-m_{a'})-m_a\widetilde{m}_b^2+m_{a'}\widetilde{m}_{b'}^2\right)+\frac{1}{8}(m_a-m_{a'})^2s\ ,\\
&\widehat{\Gamma}_{(U)0.1}{}^{abc}{}_{a'b'} = \frac{m_a^2+m_{a'}^2}{8},\quad \widehat{\Gamma}_{(U)1.0}{}^{abc}{}_{a'b'} = -\frac{m_a+m_{a'}}{8}(m_a-m_{a'})^2\ ,\quad \widehat{\Gamma}_{(U)1.1}{}^{abc}{}_{a'b'} = -\frac{m_a+m_{a'}}{8}.
\end{aligned}
\tag{18}
$$

As above, we need to introduce the linear combinations

$$
\widehat{\Gamma}_{(\mathrm{X})\pm.i}{}^{ab}{}_{a'b'c} = \widehat{\Gamma}_{(\mathrm{X})0.i}{}^{ab}{}_{a'b'c} \pm \sqrt{s}\,\widehat{\Gamma}_{(\mathrm{X})1.i}{}^{ab}{}_{a'b'c}\ , \qquad i = 0, \ldots, 3,\ X = R, S, T, U.
\tag{19}
$$

The partial waves then have the form,

$$f_{(\mathrm{vec})\ell\pm}{}^{ab}{}_{a'b'} = \frac{4\sqrt{2}G_V}{f^2} \sum_{X=R,S,T,U} \sum_{c=1}^{8} f^{cb}{}_{b'} \mathcal{X}_c{}^a{}_{a'} \widehat{f}_{(X)\ell\pm}{}^{abc}{}_{a'b'} \ , \tag{20}$$

with the reduced partial waves of (19) given by, omitting flavor indices for simplicity,

$$\widehat{f}_{(X)\ell+} = H_{(X)\ell} - \frac{1}{\ell+1} K_{(X)\ell} \ , \qquad \widehat{f}_{(X)\ell-} = H_{(X)\ell} + \frac{1}{\ell} K_{(X)\ell} \ , \tag{21a}$$

with

$$H_{(X)\ell} = \mathcal{N} \sum_{i=0}^{3} \widehat{\Gamma}_{(X)+.i} \widetilde{h}^{(\ell)}_{+.i} - \frac{\Delta t}{\mathcal{N}} \sum_{i=0}^{3} \widehat{\Gamma}_{(X)-.i} \widetilde{h}^{(\ell)}_{-.i} \ , \qquad K_{(X)\ell} = -\frac{\Delta t}{\mathcal{N}} \sum_{i=0}^{3} \widehat{\Gamma}_{(X)-.i} \widetilde{k}^{(\ell)}_{-.i} \ . \tag{21b}$$

The parameterization (17) was chosen so that the integrals $\widetilde{h}^{(\ell)}_{\pm.i}$, $\widetilde{k}^{(\ell)}_{-.i}$ appearing in (21b) can be obtained from those in (10b) by means of a substitution, as indicated in appendix B.

2.5 Partial waves from $\mathcal{O}(q^2)$ contact interactions

At low energies the meson–baryon contact vertices provide the largest contributions to the scattering amplitude. We incorporate in our Lagrangian flavor-symmetry breaking $\mathcal{O}(q^2)$ corrections to contact interactions. The $\mathcal{O}(q^2)$ Lagrangian [36] contains fifteen terms[3] out of which only three are flavor-breaking. The corresponding coupling constants are conventionally denoted $b_{0,D,F}$ [36]. The the tree-level meson–baryon scattering amplitude from these contact vertices are,

$$\begin{aligned}
\mathcal{T}_{(q^2)}{}^{ab}{}_{a'b'} &= -\frac{1}{f^2} \mathcal{F}_{(q^2)}{}^{ab}{}_{a'b'} \overline{u}' u \ , \\
\mathcal{F}_{(q^2)}{}^{ab}{}_{a'b'} &= (3b_0 + 2b_D) e^a_{a'} (\chi_0 e^b_{b'} + \chi_8 d^{8b}{}_{b'}) + \frac{2}{3} \chi_8 b_D (e^8_{b'} d^{ba}{}_{a'} + e^{8b} d_{b'}{}^a{}_{a'} + e^b_{b'} d^{8a}{}_{a'}) \\
&\quad + \frac{2}{3} \chi_8 b_F (e^8_{b'} f^{ba}{}_{a'} + e^{8b} f_{b'}{}^a{}_{a'} + e^b_{b'} d^{8a}{}_{a'}) + \sum_r 3\chi_0 d^b{}_{b'r} (b_D d^{ra}{}_{a'} + b_F f^{ra}{}_{a'}) \\
&\quad + \sum_{r,s} \chi_8 (b_D d^{ra}{}_{a'} + b_F f^{ra}{}_{a'}) (d^b{}_{b's} d^{8s}{}_r + d^8{}_{b's} d^{sb}{}_r + d^8{}_{bs} d^{sb'}{}_r) \ .
\end{aligned} \tag{22}$$

Flavor violations in the $\mathcal{O}(q^2)$ meson Lagrangian [34] are described by the matrix $\chi = 2B_0 \mathcal{M}_q$, with $\mathcal{M}_q$ the quark mass matrix and $B_0 = -\langle 0|q\overline{q}|0\rangle / f^2$ the quark condensate. In the isospin-symmetry limit $\mathcal{M}_q = \mathrm{diag}(\hat{m}, \hat{m}, m_s)$ and we can parameterize χ as,

$$\chi = \chi_0 I + \chi_8 \beta^8 \ . \tag{23}$$

This equation defines the parameters $\chi_{0,8}$ appearing in (22). At $\mathcal{O}(q^2)$ and in the isospin limit the meson [34] and baryon [36] Lagrangians lead to the relations,

$$\begin{aligned}
\widetilde{m}_b^2 &= \chi_0 + \chi_8 d^{8b}{}_b \ , \\
m_a &= M_{\mathrm{aux}} - 4b_D \chi_8 d^{8a}{}_a - 4b_F \chi_8 f^{8a}{}_a \ , \qquad M_{\mathrm{aux}} \equiv M_0 - 6b_0 \chi_0 - 4b_D \chi_0 \ ,
\end{aligned} \tag{24}$$

with M_0 on the second line being the common mass of the ground-state baryon octet in the chiral limit. These relations will be used below to fix, or estimate, the values of $\chi_{0,8}$ and $b_{0,D,F}$.

The amplitudes (22) lead to the partial waves,

$$f_{(q^2)0}{}^{ab}{}_{a'b'} = -\frac{1}{f^2} \mathcal{N} \mathcal{F}_{(q^2)}{}^{ab}{}_{a'b'} \ , \qquad f_{(q^2)1-}{}^{ab}{}_{a'b'} = \frac{1}{f^2} \frac{\Delta u}{2\mathcal{N}} \mathcal{F}_{(q^2)}{}^{ab}{}_{a'b'} \ , \tag{25}$$

with $\mathcal{N}$ defined in (9) and Δu in appendix A. All other partial waves vanish.

[3] But only seven independent combinations contribute to the meson–baryon scattering amplitude [22].

3 Unitarized partial waves

Tree-level BChPT is not sufficient by itself to describe three-flavor meson-baryon dynamics in the $S=-1$ sector, in which strong coupling effects such as subthreshold resonances render BChPT inapplicable even at threshold. We unitarize the tree-level amplitudes with the method of [15, 16]. A technically detailed explanation of the method can be found in those references. We shall limit ourselves here to stating the result of the unitarization of tree-level amplitudes.

Given a set of coupled reaction channels $|B^{a_i}M^{b_i}\rangle \to |B^{a_j}M^{b_j}\rangle$, we denote $(f_{\ell\pm})_{ij} = f_{\ell\pm}{}^{a_ib_j}{}_{a_jb_j}$ the corresponding tree-level partial-wave matrix. A solution to the unitarity equation for T, resumming the right-hand cut in the s-plane, is given by the partial waves $(\mathcal{F}_{\ell\pm})_{ij}$ related to $(f_{\ell\pm})_{ij}$ by the matrix equation,

$$\mathcal{F}_{\ell\pm} = (I + f_{\ell\pm}\cdot G)^{-1}\cdot f_{\ell\pm}\ , \tag{26}$$

where I is an identity matrix, and G is the diagonal matrix $G_{ij} = g^{a_ib_i}\delta_{ij}$ (no summation over i, j). The "unitarity bubbles" g^{ab} are given by,

$$\begin{aligned} g^{ab}(s) &= \frac{i\mu^\epsilon}{(2\pi)^d}\int d^dk \frac{1}{(k^2-m^2+i0)((k+p_T)^2-m_a^2+i0)} \quad + \text{ counterterm} \\ &= \frac{1}{16\pi^2}\left\{a^{ab} + \log\left(\frac{m_a^2}{\mu^2}\right) + \frac{s-m_a^2+\widetilde{m}_b^2}{2s}\log\left(\frac{\widetilde{m}_b^2}{m_a^2}\right) + \frac{w(s,m_a^2,\widetilde{m}_b^2)}{2s}\times\right. \\ &\left.\times\left\{\left[\log\left(\frac{m_a^2-\widetilde{m}_b^2-s-w(s,m_a^2,\widetilde{m}_b^2)}{2s}-i0\right) - \log\left(\frac{m_a^2-\widetilde{m}_b^2-s+w(s,m_a^2,\widetilde{m}_b^2)}{2s}+i0\right)\right]\right\}\right\}\ , \end{aligned} \tag{27}$$

with $w(x,y,z)$ defined in appendix A. The loop function g^{ab} was computed in (27) in dimensional regularization. The subtraction constants a^{ab}, depending on the renormalization scale μ, are taken as free parameters in each isospin channel. Variations in μ can be offset by a redefinition of a^{ab} [15].

4 Results

In this section we discuss our results for the reactions $pK^- \to B^{a'}M^{b'}$. Within the range of initial-meson momentum $0 \le q_{\rm lab} \lesssim 600$ MeV considered here the only possible final states are $N\overline{K}$, $\Lambda\pi$, $\Sigma\pi$. Following [10, 16, 20, 50], however, we apply the unitarization method of [15, 16] including as intermediate states also $\Lambda\eta$, $\Sigma\eta$, ΞK. This is justified by the fact that in lowest-order BChPT those states are degenerate. The contribution of D waves is obviously important in the region around and above the $\Lambda(1520)$ resonance, but F waves are negligible for $q_{\rm lab} \lesssim 800$ MeV. Thus, we compute physical observables from $S_{1/2}$, $P_{1/2}$, $P_{3/2}$, $D_{3/2}$ and $D_{5/2}$ partial waves obtained from ten-channel unitarization of tree-level partial waves.

The baryon nonet requires separate consideration. We find that it is not possible, as pointed out in [13], to fit experimental data if partial waves from nonet-baryon exchange other than $D_{3/2}$ are included. This is undoubtedly a reflection of nonet resonances being dynamical in nature, or at least possessing a significant dynamical component. Unlike [13], however, we find that by including both the s and u channels we get somewhat lower χ^2 values than by dropping the u-channel contribution. We therefore take into account only the $D_{3/2}$ wave in nonet-baryon exchange amplitudes, but retain both s- and u-channel contributions to it. As a consequence, the parameter κ_9 does play a role in our fits.

The experimental data included in our fits consists of about 2800 points comprising the threshold branching fractions γ, R_c and R_n [51, 52], total [53–59] and differential [54, 56] cross section data for the six open reactions channels up to $q_{\rm lab} \lesssim 600$ MeV, and the first two Legendre moments of the CM-frame differential cross sections and spin asymmetries for $pK^- \to \Sigma\pi, \Lambda\pi$ [55, 57, 58]. In the figures below we display also higher-energy cross-section data from those references and from [60,61], and CM-frame spin asymmetry data from [54], which were not included in our fits.

4.1 Fitting procedure and parameters

For numerical computations we set meson and baryon masses to their physical values [24]. Following [16,20], below we set $\mu = 630$ MeV. The coupling constants for the ground-state baryon and meson octet vertices have been computed from semileptonic hyperon decays [62, 63]. We keep them fixed at the values $D = 0.80$

and $F = 0.46$, which are consistent with [63] and with the tree-level results of [62]. The coupling constants for the nonet of baryon resonances can be obtained from a flavor SU(3) analysis of their tree-level strong decay widths [13, 64]. Since, however, in our treatment those resonances acquire their widths dynamically through the loop corrections involved in unitarization, we take their couplings as free parameters in our fits.

In order to obtain a picture of the role played by the different interactions described in sect. 2, we present below results from three different fits to data. First, we consider scattering amplitudes obtained from the ground-state baryon–pseudoscalar meson $\mathcal{O}(q^1)$ contact interaction, and from s- and u-channel exchange of octet, decuplet and nonet baryons. The best fit obtained with those amplitudes is referred to below as "fit III." Second, a different series of fits is obtained by augmenting the previous amplitudes by t-channel vector-meson exchange. For these fits we take the coupling-constant products $G_V X_{D,F}$, in the notation of sect. 2.4, as free parameters. The best of those fits is denoted "fit II" below.

Finally, we report on another series of fits obtained by adding to the amplitudes of fit II the $\mathcal{O}(q^2)$ flavor-symmetry breaking corrections to baryon–meson contact vertices. The LECs in the $\mathcal{O}(q^2)$ amplitudes of sect. 2.5 are related to pseudoscalar meson masses and ground-state baryon mass splittings. Fitting the expression for meson masses (24) to data [24] we obtain

$$\chi_0 = (412.04\ \text{MeV})^2\ , \qquad \chi_8 = -(510.54\ \text{MeV})^2\ . \tag{28}$$

We keep $\chi_{0,8}$ fixed to these values in our fits, which actually implies no restriction since in the flavor-breaking $\mathcal{O}(q^2)$ contact interactions, couplings always appear in the combinations $\chi_i b_j$ with $i = 0, 8$, $j = 0, D, F$. The couplings $b_{0,D,F}$ can then be either treated as free parameters in our partial waves or, alternatively, fixed from baryon mass data. Fitting the baryon masses in (24) to experimental data [24] with $M_{\rm aux}$, $b_{D,F}$ as parameters we get

$$M_0 - 6\chi_0 b_0 = 1110.61\ \text{MeV}\ , \qquad b_D = 6.51\times 10^{-5}\ \text{MeV}^{-1}\ , \qquad b_F = -2.17\times 10^{-4}\ \text{MeV}^{-1}\ . \tag{29}$$

This equation does not completely fix b_0 due to the uncertainty in M_0, with $-3\times 10^{-4} < b_0 < -2\times 10^{-4}$ MeV^{-1} for $800 < M_0 < 900$ MeV. We call "fit I" the best fit obtained by setting $b_{D,F}$ to the values (29), and taking b_0 as a free parameter constrained to the range (-3)—(-2) $\times 10^{-4}$ MeV^{-1}. As pointed out in [22], however, because unitarization resums an infinite sequence of diagrams, the numerical values for $b_{0,D,F}$ we obtain in UBChPT need not be the same as those obtained in fixed-order BChPT. Thus, we also performed a fit with freely varying $b_{0,D,F}$, referred to as "fit I′". As discussed below, the numerical values for $b_{0,D,F}$ obtained in fit I′ are close to those of I, and the plots of fits I and I′ are virtually identical.

A summary of our best-fit parameters is as follows.

Fit I $f = 90.82$ MeV, $b_0 = -3.0\times 10^{-4}$ MeV^{-1},

Subtraction constants:

$$a^{N\overline{K}} = -1.83,\ a^{\Lambda\pi} = -2.14,\ a^{\Sigma\pi} = -0.63,\ a^{\Lambda\eta} = -1.75,\ a^{\Sigma\eta} = -2.14,\ a^{\Xi K} = -1.41\ .$$

Decuplet and nonet parameters:

$$g_{10} = 0.89,\ \kappa = -0.32,\ D_0 = 1.68,\ D_8 = 0.20,\ F_8 = 1.59,\ \kappa_9 = 2.49,\ \theta = -0.33\ .$$

Vector-meson couplings: $[R_{D,F}] = 1$, $[S_{D,F}] = \text{MeV}^{-1}$, $[T_{D,F}] = \text{MeV}^{-3}$, $[U_{D,F}] = \text{MeV}^{-2}$,

$$G_V R_D = 52.76,\ G_V R_F = 75.42,\ G_V S_D = 0.16,\ G_V S_F = 0.036,$$
$$G_V T_D = 1.23\times 10^{-6},\ G_V T_F = -1.36\times 10^{-7},\ G_V U_D = 1.27\times 10^{-4},\ G_V U_F = 1.37\times 10^{-4}\ .$$

Fit I′ $f = 91.42$ MeV,

Subtraction constants:

$$a^{N\overline{K}} = -1.84,\ a^{\Lambda\pi} = -1.72,\ a^{\Sigma\pi} = -0.70,\ a^{\Lambda\eta} = -1.70,\ a^{\Sigma\eta} = -2.15,\ a^{\Xi K} = -0.78\ .$$

Decuplet and nonet parameters:

$$g_{10} = 0.90,\ \kappa = -0.31,\ D_0 = 1.65,\ D_8 = -0.03,\ F_8 = 1.89,\ \kappa_9 = 2.31,\ \theta = -0.34\ .$$

Vector-meson couplings: $[R_{D,F}] = 1$, $[S_{D,F}] = \text{MeV}^{-1}$, $[T_{D,F}] = \text{MeV}^{-3}$, $[U_{D,F}] = \text{MeV}^{-2}$,

$$G_V R_D = 52.87,\ G_V R_F = 68.75,\ G_V S_D = 0.19,\ G_V S_F = 0.022,$$
$$G_V T_D = 9.83 \times 10^{-7},\ G_V T_F = -4.96 \times 10^{-8},\ G_V U_D = 1.46 \times 10^{-4},\ G_V U_F = 2.00 \times 10^{-4}\ .$$

$\mathcal{O}(q^2)$ contact interaction couplings: [MeV^{-1}]

$$b_0 = -4.0 \times 10^{-4}, \quad b_D = 1.45 \times 10^{-4}, \quad b_F = -2.38 \times 10^{-4}\ .$$

Fit II $f = 95.97$ MeV,

Subtraction constants:

$$a^{N\overline{K}} = -1.84,\ a^{\Lambda\pi} = -3.31,\ a^{\Sigma\pi} = -0.41,\ a^{\Lambda\eta} = -3.28,\ a^{\Sigma\eta} = -2.54,\ a^{\Xi K} = -1.15\ .$$

Decuplet and nonet parameters:

$$g_{10} = 0.87,\ \kappa = -0.34,\ D_0 = 1.68,\ D_8 = -0.038,\ F_8 = 1.84,\ \kappa_9 = 2.28,\ \theta = -0.31\ .$$

Vector-meson couplings: $[R_{D,F}] = 1$, $[S_{D,F}] = \text{MeV}^{-1}$, $[T_{D,F}] = \text{MeV}^{-3}$, $[U_{D,F}] = \text{MeV}^{-2}$,

$$G_V R_D = 57.90,\ G_V R_F = 89.91,\ G_V S_D = 3.66 \times 10^{-3},\ G_V S_F = -0.12,$$
$$G_V T_D = 5.27 \times 10^{-7},\ G_V T_F = -5.0 \times 10^{-7},\ G_V U_D = -1.70 \times 10^{-5},\ G_V U_F = 1.20 \times 10^{-4}\ .$$

Fit III $f = 95.81$ MeV,

Subtraction constants:

$$a^{N\overline{K}} = -1.68,\ a^{\Lambda\pi} = -2.16,\ a^{\Sigma\pi} = -0.82,\ a^{\Lambda\eta} = -3.85,\ a^{\Sigma\eta} = -2.56,\ a^{\Xi K} = -1.27\ .$$

Decuplet and nonet parameters:

$$g_{10} = 0.83,\ \kappa = -0.28,\ D_0 = 1.73,\ D_8 = 0.20,\ F_8 = 1.74,\ \kappa_9 = 2.30,\ \theta = -0.17\ .$$

Some remarks about these parameters are in order. The subtraction constants show less dispersion about their "natural" dimensional regularization value -2 [16] in fits I and I′ than in fit II, which shows less dispersion than III. Most of the parameters are quite stable across fits, with the exception of D_8, θ and $G_V S_{D,F}$ which show larger variations. Other determinations of $b_{0,D,F}$ from fits to pK^- data are given in [13, 22], with results quite similar to ours.

The values for the nonet couplings D_0, D_8, F_8 are similar to those expected from the flavor symmetry analysis of decay widths of [64], as updated in [13]: 1.57, 0.59, 1.27, resp., with D_8 showing the largest departures. The values for θ we obtain are in general agreement with the observation that $\Lambda(1520)$ is predominantly a flavor singlet. For fits I, I′ and II we get $\theta \simeq -20^o$ to be compared with the value -28^o adopted in [13]. As remarked above, the nonet parameters reported here differ from those computed in [13,64] by loop corrections, so numerical equality among them is not expected.

A direct comparison of our numerical results for vector-meson couplings in three-flavor UBChPT to those of the two-flavor analysis of pion–nucleon scattering of [15] would not be meaningful. It is nevertheless interesting to find out where our results stand relative to those of [15]. Assuming $G_V = 60$ MeV, from [15] we find,

$$\begin{gathered} G_V(R_D + R_F) \simeq 312 \text{ MeV}\ , \quad G_V(S_D + S_F - \frac{m_N}{2}(U_D + U_F)) \simeq 3.3 \times 10^{-1}\ , \\ 6 \times 10^{-7} \lesssim G_V(T_D + T_F) \lesssim 1.8 \times 10^{-6} \text{ MeV}^{-2}\ . \end{gathered} \tag{30}$$

From our fit I we get $G_V(R_D + R_F) = 128.2$ MeV, $G_V(T_D + T_F) = 1.1 \times 10^{-6}$ MeV^{-2}, which are of the same order of magnitude as (30), and $G_V(S_D + S_F - \frac{m_N}{2}(U_D + U_F)) = 2.1 \times 10^{-2}$ which is an order of magnitude smaller than the value in (30). This latter result, however, arises from a numerical cancellation between the two terms and is therefore rather fortuitous. Indeed, we could fine-tune the couplings $U_{D,F}$ in our fit so as to lead to a larger value roughly in agreement with (30) without appreciably changing the fit results. As is easy to check, fit I′ leads to the same conclusions. From fit II we get, $G_V(R_D + R_F) = 147.8$ MeV, $G_V(T_D + T_F) = 2.7 \times 10^{-8}$ MeV^{-2} and $G_V(S_D + S_F - \frac{m_N}{2}(U_D + U_F)) = 1.7 \times 10^{-1}$. Whereas in all our type-I fits we find $-T_F \ll T_D$, in our type-II fits we systematically obtain $-T_F \sim T_D$, causing $G_V(T_D + T_F)$ to be small compared to (30).

4.2 Physics results

For fit I we get the threshold branching fractions (defined in App. C) $\gamma = 2.35$ (2.36 ± 0.04), $R_c = 0.645$ (0.664 ± 0.011), $R_n = 0.210$ (0.189 ± 0.015), in good agreement with the experimental values [51, 52] quoted in parentheses. Fits I′, II and III lead to essentially the same results. We computed also the scattering length a_{K^-p} (see App. C) for the elastic process at threshold, which is not included in our fits. From fit I we get $a_{K^-p} = -1.09 + 0.63i$ fm, with the other fits showing only variations in the second decimal. This value for a_{K^-p} is in reasonable agreement with the KEK result [65, 66], $a_{K^-p} = (-0.78 \pm 0.15 \pm 0.03) + i(0.49 \pm 0.25 \pm 0.12)$ fm, but significantly larger than the DEAR one [67], $a_{K^-p} = (-0.468 \pm 0.09 \pm 0.015) + i(0.302 \pm 0.135 \pm 0.036)$ fm. The issue of the (in)consistency of the DEAR measurement with the previous KEK one and with other hadronic data is beyond the scope of this paper; it has been discussed in detail in [22, 68–71] and references cited there.

We present our results for cross sections and spin asymmetries in the figures below. For clarity, we omit plotting fit I′ in the figures, since its curves are almost indistinguishable from fit I. Fig. 1 shows our results for total cross sections. Fits I and II give a very good description of data, while fit III is somewhat less accurate, especially in the region of the $\Lambda(1520)$ peak where it tends to overshoot the data in $\Sigma\pi$ channels. All three fits, and a large number of other fits we have conducted, underestimate the $\Sigma^0\pi^0$ cross section for $q_{\rm lab} < 350$ MeV. We cannot explain this phenomenon, which is also present to different extents in [13, 20, 23].

We included all data for differential cross sections from [54, 56] up to $q_{\rm lab} = 600$ MeV in our fits, though some higher energy data is also shown fig. 2. Given the large number of data points reported in [54, 56], only a representative selection of results is shown in the figure. The overall agreement of fits I and II with data is excellent, while fit III provides a less accurate though still reasonably good description. For all three fits the agreement with data is better for charged-baryon final states than for neutral ones. As seen in the figure, for charged-baryon channels even data with $q_{\rm lab}$ over 600 MeV is well reproduced by fits I and II.

In fig. 3 we show our results for Legendre moments of differential cross sections and of CMF spin asymmetries normalized to A_0 (see App. C for definitions). We omit the moments for processes with nucleon final states because very detailed data on differential cross sections for them has already been included in our fits. For the processes with hyperon final states shown in the figure we restrict ourselves to the first two moments, $A_{1,2}$ and $B_{1,2}$, since higher-order ones have rather small values and large experimental errors which make them consistent with zero throughout the energy range. The experimental data on those moments are displayed in the figure without modification. Thus, to match the experimentally measured quantities, the moments $B_{1,2}$ computed with our unitarized amplitudes are multiplied by the final-state baryon polarizabilities α reported in [24]. As seen in fig. 3, the data for most processes have small errors in the region of the $\Lambda(1520)$ resonance, providing a good constraint to fit parameters. The agreement with data is globally very good, especially for the charged modes $pK^- \to \Sigma^\pm\pi^\mp$. Fits I and II accurately reproduce the structures in the data around the $\Lambda(1520)$ peak. For the moment B_1 in $pK^- \to \Lambda\pi^0$ all three fits yield positive values at lower energies, with a negative slope, whereas as remarked in [23], both [13, 23] obtain negative values for that moment.

Fig. 4 shows our results for the CMF final-state spin asymmetry. The asymmetry data were not included in our fits due to their rather large experimental errors. In that sense, these results are "predictions" of the theory. Interestingly, for this observable the three fits show some of the largest differences among them. Thus, more precise data on spin asymmetry, polarization or analyzing power could provide some of the most discriminating and stringent tests of the theory. As seen in the figure, within experimental errors all three fits describe the data very well at all energies. Since these data were not fitted, such agreement is non-trivial.

Finally, in fig. 5 we display the $\Sigma\pi$ mass distribution computed from the isoscalar components of the amplitudes for $N\overline{K} \to \Sigma\pi$ and $\Sigma\pi \to \Sigma\pi$ in $S_{1/2}$ wave, and for $N\overline{K} \to \Sigma\pi$ in $D_{3/2}$ wave. From the $S_{1/2}$ wave we obtain the mass spectrum for the resonance $\Lambda(1405)$, dynamically generated by unitarization [10,13,16,20], which is well known to be process dependent. That dependence can in principle be understood from the two-pole structure of this resonance [21]. The spectra plotted in the figure are consistent with those of [21] (see fig. 4 of that ref. See also, e.g., figs. 9 of [13] and 2 of [10]). Averaging the results from the three fits, we obtain a resonance peak at 1409.7 ± 1.5 MeV with a width of 20.2 ± 0.5 MeV for the $\Sigma\pi \to \Sigma\pi$ channel, and a peak at 1414.7 ± 1 MeV with a width of 20 ± 1 MeV for the $N\overline{K} \to \Sigma\pi$ channel. Similarly, from the $D_{3/2}$ wave we obtain the mass spectrum for $\Lambda(1520)$. Again averaging the results from the three fits, we obtain a resonance peak at 1518.5 ± 0.5 MeV and a width of 14.1 ± 0.8 MeV, which are in excellent agreement with the measured values [24] if we take into account that three-body decay modes not considered here constitute 11% of the full experimental width.

In summary, an excellent global description of pK^- scattering data is obtained with fits I and II, up to $q_{\rm lab} \lesssim 600$ MeV, and including threshold observables. Fit III is in very good agreement with data up to $q_{\rm lab} \lesssim 350$ MeV, but provides a weaker description of data in the region of the $\Lambda(1520)$ peak and above. Vector-meson interactions play an important role in the theoretical description, leading to a decrease of $\sim 25\%$ in the global χ^2 of fit II with respect to III, and to an improved description of the data in the $\Lambda(1520)$ region as can be seen in the figures. Inclusion of $\mathcal{O}(q^2)$ flavor-breaking contact interactions leads to some additional, though less marked, improvements reflected in a further decrease of $\sim 5\%$ in the global χ^2. Experimental results can be theoretically reproduced only if nonet baryon resonance exchange is restricted to the $D_{3/2}$ wave, which is strong evidence that those resonances are produced by the coupled-channel dynamics or, at least, possess a large dynamical component. Whereas the global agreement with data is remarkably good, there are differences in detail between theory and data, especially in reaction channels with a neutral final baryon, and in most channels at momenta $q_{\rm lab} \gtrsim 600$. We attribute those differences mostly to the contribution of processes with two final mesons, particularly $pK^- \to \Sigma^0\pi^0\pi^0$, which are not included in our treatment.

5 Final remarks

In the previous sections we presented a detailed study of two-body polarized pK^- scattering in the energy range from threshold through the $\Lambda(1520)$ peak, $0 \leq q_{\rm lab} \lesssim 600$ MeV, in UBChPT. Our results show excellent global agreement with experimental data. This is achieved by taking into account ground-state baryon and meson interactions, including flavor-breaking contact interactions of $\mathcal{O}(q^2)$, as well as $J^P = 3/2^+$ decuplet and $3/2^-$ nonet exchange in s- and u-channels, and t-channel vector-meson exchange. Notice that the latter has not been considered in previous treatments of pK^- scattering in UBChPT. Whereas scattering amplitudes involving solely pseudoscalar mesons yield good semiquantitative agreement with data, inclusion of vector-meson exchange diagrams leads to an improved quantitative description. Further small improvements are also obtained from the flavor-breaking contact interactions. The five partial waves $S_{1/2}$, $P_{1/2}$, $P_{3/2}$, $D_{3/2}$, $D_{5/2}$ were taken into account in all amplitudes, with the exception of baryon nonet exchange ones. The fact that it is necessary to exclude all waves but $D_{3/2}$ of nonet-mediated diagrams originates most certainly in the large dynamical component of $J^P = 3/2^-$ resonances reported in the literature.

From the theoretical point of view, we report explicit expressions for partial waves for s- and u-channel baryon, and for t-channel vector-meson, exchange diagrams not given in the previous literature. From a phenomenological point of view, an improvement with respect to previous global analyses of pK^- low-energy data is our inclusion of differential cross-section data in the region of the $\Lambda(1520)$ resonance and above. Our fits describe the data remarkably well, including measured threshold parameters, total and differential cross-section data, and spin asymmetries. A noteworthy example is the description of the CMF spin asymmetry (in the form of Legendre moments, see fig. 3) around the $\Lambda(1520)$ peak, which also shows the important role played by vector meson interactions. Very good agreement is also obtained with the spin asymmetry data shown in fig. 4, although those data were not included in the fit. As seen in figs. 3 and 4, spin observables are quite discriminating among different fits. More precise spin-asymmetry data would be theoretically most desirable and challenging. For the fitted couplings and, especially, subtractions constants we obtain more natural values than in our previous lower-energy treatment [23]. A further improvement in the analysis, and an extension in its energy range, should be made possible by the addition of further reaction channels to the unitarization procedure, particularly three-body processes. Work along those lines is currently in progress.

Acknowledgements

The author gratefully acknowledges access to the computer "KanBalam" granted to him by Departamento de Supercómputo, Dirección General de Servicios de Cómputo Académico, Universidad Nacional Autónoma de México.

References

[1] V. Bernard, U. G. Meissner, Annu. Rev. Nucl. Part. Sci. **57** (2007) 33.

[2] B. Borasoy, *Introduction to Chiral Perturbation Theory,* Lectures given at the 2nd Summer School on Particle Accelerators and Detectors, Bodrum, Turkey, Sep. 2006; arXiv:hep-ph/0703297.

[3] S. Scherer, M. R. Schindler, *A Chiral Perturbation Theory Primer,* lectures given at the European Centre for Theoretical Studies in Nuclear Physics and Related Areas, Trento, Italy, 2005; arXiv:hep-ph/0505265.

[4] S. Weinberg, *The Quantum Theory of Fields*, Vol. II, Cambridge Univ. Press, New York, 1996.

[5] J. F. Donoghue, E. Golowich, B. R. Holstein, *Dynamics of the Standard Model,* Cambridge Univ. Press, New York, 1994.

[6] V. Bernard, Prog. Part. Nucl. Phys. **60** (2008) 82.

[7] P. Siegel, W. Weise, Phys. Rev. C **38** (1988) 2221.

[8] N. Kaiser, P. B. Siegel, W. Weise, Phys. Lett. B **362** (1995) 23.

[9] N. Kaiser, T. Waas, W. Weise, Nucl. Phys. A **612** (1997) 297.

[10] E. Oset, A. Ramos, Nucl. Phys. A **635** (1998) 99.

[11] B. Krippa, Phys. Rev. C **58** (1998) 1333.

[12] B. Krippa, J. Londergan, Phys. Rev. C **58** (1998) 1634.

[13] M. F. M. Lutz, E. Kolomeitsev, Nucl. Phys. A **700** (2002) 193.

[14] B. Borasoy, E. Marco, S. Wetzel, Phys. Rev. C **66** (2002) 055208.

[15] U. G. Meissner, J. A. Oller, Nucl. Phys. A **673** (2000) 311.

[16] J. A. Oller, U. G. Meissner, Phys. Lett. B **500** (2001) 263.

[17] G. F. Chew, S. Mandelstam, Phys. Rev. **119** (1960) 467.

[18] J. A. Oller, E. Oset, J. R. Peláez, Phys. Rev. D **59** (1999) 074001.

[19] J. A. Oller, E. Oset, Phys. Rev. D **60** (1999) 074023.

[20] D. Jido, E. Oset, A. Ramos, Phys. Rev. C **66** (2002) 055203.

[21] D. Jido, J. A. Oller, E. Oset, A. Ramos, U.-G. Meissner, Nucl. Phys. A **725** (2003) 181.

[22] J. A. Oller, Eur. Phys. J. A **28** (2006) 63.

[23] A. O. Bouzas, Eur. Phys. J. A **37** (2008) 201.

[24] Particle Data Group: C. Amsler et al., Phys. Lett. B **667** (2008).

[25] E. Oset, A. Ramos, C. Bennhold, Phys. Lett. B **527** (2002) 99.

[26] S. Sarkar, E. Oset, M. J. Vicente Vacas, Nucl. Phys. A **750** (2005) 294. Erratum: ibid. **780** (2006) 89.

[27] M. F. M. Lutz, G. Wolf, B. Friman, Nucl. Phys. A **661** (1999) 526.

[28] T. Inoue, E. Oset, M. J. Vicente Vacas, Phys. Rev. C **65** (2002) 035204.

[29] M. F. M. Lutz, E. E. Kolomeitsev, Nucl. Phys. A **755** (2005) 29.

[30] A. Ramos, V. K. Magas, T. Mizutani, E. Oset, L. Tolos, *Resonances in chiral unitary approaches*, paper contributed to the "Workshop on the Physics of Excited Nucleons" (NSTAR 2007), Bonn, Germany, Sep. 2007, and arXiv:0711.4042.

[31] E. Oset et al., *Dynamically generated resonances,* talk given at "Workshop on the Physics of Excited Nucleon" (NSTAR 2009), Beijing, China, Apr. 2009, and arXiv:0906.3801.

[32] D. Jido, M. Doering, E. Oset, Phys. Rev. C **77** (2008) 065207.

[33] T. Hyodo, D. Jido, A. Hosaka, Phys. Rev. C **78** (2008) 025203.

[34] J. Gasser, H. Leutwyler, Ann. Phys. (N.Y.) **158** (1984) 142.

[35] J. Gasser, H. Leutwyler, Nucl. Phys. B **250** (1985) 465.

[36] J. A. Oller, J. Prades, M. Verbeni, J. High Energy Phys. **0609** (2006) 079.

[37] A. Krause, Helv. Phys. Acta **63** (1990) 3.

[38] B. Borasoy, U.-G. Meissner, Ann. Phys. **254** (1997) 192.

[39] M. Frink, U. G. Meissner, J. High Energy Phys. **0407** (2004) 028.

[40] J. Gasser, M. E. Sainio, A. Svarc, Nucl. Phys. **B 307** (1988) 779.

[41] A. Bouzas, Int. J. Mod. Phys. E **17** (2008) 1477.

[42] V. Bernard, N. Kaiser, U.-G. Meissner, Int. J. Mod. Phys. E **4** (1995) 193.

[43] M. Benmerrouche, R. M. Davidson, N. C. Mukhopadhyay, Phys. Rev. C **39** (1989) 2339.

[44] M. G. Olsson, E. T. Osypowski, E. H. Monsay, Phys. Rev. D **17** (1978) 2938.

[45] V. Pascalutsa, M. Vanderhaeghen, S. N. Yang, Phys. Rep. 437 (2007) 125.

[46] R. F. Lebed, Nucl. Phys. B **430** 1994 295.

[47] H. Krebs, E. Epelbaum, U.-G. Meissner, *Redundancy of the off-shell parameters in chiral effective field theory with explicit spin-3/2 degrees of freedom,* arXiv:0905.2744.

[48] G. Ecker, J. Gasser, H. Leutwyler, A. Pich, E. de Rafael, Phys. Lett. B **223** (1989) 425.

[49] B. Borasoy, U.-G. Meissner, Int. J. Mod. Phys. A **11** (1996) 5183.

[50] E. Oset, A. Ramos, C. Bennhold, Phys. Lett. B **527** (2002) 99. Erratum: ibid. **530** (2002) 260.

[51] D. Tovee et al., Nucl. Phys. B **33** (1971) 493.

[52] R. Novak et al., Nucl. Phys. B **139** (1978) 61.

[53] M. Sakitt et al., Phys. Rev. **139** (1965) B719.

[54] R. Armenteros et al., Nucl. Phys. B **21** (1970) 15.

[55] T. S. Mast et al., Phys. Rev. D **11** (1975) 3078.

[56] T. S. Mast et al., Phys. Rev. D 14 (1976) 13.

[57] R. O. Bangerter et al., Phys. Rev. D **23** (1981) 1484.

[58] J. Ciborowski et al., J. Phys. G **8** (1982) 13.

[59] D. Evans et al., J. Phys. G **9** (1983) 885.

[60] C. J. Adams et al., Nucl. Phys. B **96** (1975) 54.

[61] M. Alston-Garnjost et al., Phys. Rev. D **17** (1978) 2216.

[62] B. Borasoy, Phys. Rev. D **59** (1999) 054021.

[63] P. G. Ratcliffe, Phys. Rev. D **59** (1999) 014038.

[64] D. E. Plane et al., Nucl. Phys. B **22** (1970) 93.

[65] M. Iwasaki et al., Phys. Rev. Lett. **78** (1997) 3067.

[66] T. M. Ito et al., Phys. Rev. C **58** (1998) 2366.

[67] G. Beer et al., Phys. Rev. Lett. **94** (2005) 212302.

[68] U.-G. Meissner, U. Raha, A. Rusetsky, Eur. Phys. J. C **35** (2004) 349.

[69] B. Borasoy, R. Nissler, W. Weise, Phys. Rev. Lett. **94** (2005) 213401.

[70] J. A. Oller, J. Prades, M. Verbeni, Phys. Rev. Lett. **95** (2005) 172502.

[71] B. Borasoy, R. Nissler, W. Weise, Eur. Phys. J. A**25** (2005) 79.

[72] M. Abramowitz, I. Stegun, *Handbook of Mathematical Functions,* Dover Pub., New York, 1972.

A Kinematics

In this appendix we gather some kinematical definitions used throughout the paper. We introduce the notation

$$\omega(x,y,z) = (x^2+y^2+z^2-2xy-2xz-2yz)^{\frac{1}{2}} = (x-(\sqrt{y}+\sqrt{z})^2)^{\frac{1}{2}}(x-(\sqrt{y}-\sqrt{z})^2)^{\frac{1}{2}} \ . \tag{A.1}$$

The function ω appears frequently in relativistic kinematics (*e.g.,* in the center of mass frame $|\vec{p}| = \omega(s,m_a^2,\widetilde{m}_b^2)/(2\sqrt{s})$). The Mandelstam invariants for the process $|B^a(p,\sigma)M^b(q)\rangle \longrightarrow |B^{a'}(p',\sigma')M^{b'}(q')\rangle$ are

$$s=(p+q)^2=(p'+q')^2 \ , \quad t=(p-p')^2=(q-q')^2 \ , \quad u=(p-q')^2=(p'-q)^2 \ , \tag{A.2}$$

with $s+t+u = m_a^2+m_{a'}^2+\widetilde{m}_b^2+\widetilde{m}_{b'}^2$. The physical region for the process is defined by the inequalities

$$s_{\rm th} \le s \ , \quad t_{\rm min} \le t \le t_{\rm max} \ , \quad u_{\rm min} \le u \le u_{\rm max} \ , \tag{A.3}$$

where,

$$\begin{aligned}
s_{\rm th} &= \max\left\{(m_a+\widetilde{m}_b)^2,(m_{a'}+\widetilde{m}_{b'})^2\right\} \\
t_{\rm \substack{max\\min}} &= -\frac{1}{2s}\Big(s^2-s(m_a^2+m_{a'}^2+\widetilde{m}_b^2+\widetilde{m}_{b'}^2)+(m_a^2-\widetilde{m}_b^2)(m_{a'}^2-\widetilde{m}_{b'}^2)\Big) \\
&\quad \pm \frac{1}{2s}\omega(s,m_a^2,\widetilde{m}_b^2)\omega(s,m_{a'}^2,\widetilde{m}_{b'}^2), \\
u_{\rm \substack{max\\min}} &= -\frac{1}{2s}\Big(s^2-s(m_a^2+m_{a'}^2+\widetilde{m}_b^2+\widetilde{m}_{b'}^2)-(m_a^2-\widetilde{m}_b^2)(m_{a'}^2-\widetilde{m}_{b'}^2)\Big) \\
&\quad \pm \frac{1}{2s}\omega(s,m_a^2,\widetilde{m}_b^2)\omega(s,m_{a'}^2,\widetilde{m}_{b'}^2).
\end{aligned} \tag{A.4}$$

We introduce also the following useful notations,

$$\langle u\rangle = \frac{u_{\rm max}+u_{\rm min}}{2} \ , \quad \langle t\rangle = \frac{t_{\rm max}+t_{\rm min}}{2} \ , \quad \Delta u = \frac{u_{\rm max}-u_{\rm min}}{2} = \frac{t_{\rm max}-t_{\rm min}}{2} = \Delta t \ . \tag{A.5}$$

As is easy to check, $s+\langle t\rangle+\langle u\rangle = m_a^2+m_{a'}^2+\widetilde{m}_b^2+\widetilde{m}_{b'}^2$ and, in the CMF,

$$u = \langle u\rangle - x\Delta u \ , \quad t = \langle t\rangle + x\Delta t \ , \quad x \equiv \widehat{p}'\cdot\widehat{p} \ . \tag{A.6}$$

In the laboratory frame we have, in terms of Mandelstam invariants,

$$q^0_{\rm lab} = \frac{1}{2m_a}(s-m_a^2-\widetilde{m}_b^2), \quad q'^0_{\rm lab} = \frac{1}{2m_a}(m_a^2+\widetilde{m}_{b'}^2-u), \quad p'^0_{\rm lab} = \frac{1}{2m_a}(m_a^2+m_{a'}^2-t), \tag{A.7a}$$

therefore,

$$q_{\rm lab} \equiv |\vec{q}_{\rm lab}| = \frac{1}{2m_a}\omega(s,m_a^2,\widetilde{m}_b^2), \quad |\vec{q}\,'_{\rm lab}| = \frac{1}{2m_a}\omega(u,m_a^2,\widetilde{m}_{b'}^2), \quad |\vec{p}\,'_{\rm lab}| = \frac{1}{2m_a}\omega(t,m_a^2,m_{a'}^2). \tag{A.7b}$$

B Partial-wave integrals

The integrals of Legendre polynomials $P_\ell(x)$, and their derivatives, involved in the expression of partial waves in (10) and (21) are listed in this appendix. For decuplet baryons M_C denotes the mass of the $C^{\rm th}$ member of the decuplet, $C=1,\ldots,10$. We denote also,

$$z_C = \frac{M_C^2-\langle u\rangle}{\Delta u} \ , \tag{B.1}$$

with $\langle u\rangle$, Δu defined in appendix A. In what follows, $Q_\ell(z)$ denotes the Legendre function of the second kind [72], analytic on the z plane cut along $-1<z<1$ for ℓ a nonnegative integer. When analytic continuation is necessary (e.g., if $-1<z_C<1$ in the expressions below) the mass M_C should be understood as M_C-i0. The invariants u and t are given as functions of $x=\cos\theta_{CM}$ in (A.6).

$$h^{(\ell)}_{+.0} = \int_{-1}^{1} dx\,\frac{1}{u-M_C^2}P_\ell(x) = \frac{(-1)^{\ell+1}}{\Delta u}Q_\ell(z_C) \tag{B.2}$$

$$h^{(\ell)}_{+.1} = \int_{-1}^{1} dx\, \frac{u}{u-M_C^2} P_\ell(x) = (-1)^{\ell+1}\left(\frac{M_C^2}{\Delta u} Q_\ell(z_C) - \delta_{\ell 0}\right) \tag{B.3}$$

$$h^{(\ell)}_{+.2} = \int_{-1}^{1} dx\, \frac{u^2}{u-M_C^2} P_\ell(x) = (-1)^{\ell+1}\left(\frac{(\langle u\rangle + z_C\Delta u)^2}{\Delta u} Q_\ell(z_C) - (2\langle u\rangle + z_C\Delta u)\delta_{\ell 0} - \frac{\Delta u}{3}\delta_{\ell 1}\right) \tag{B.4}$$

$$h^{(\ell)}_{+.3} = \int_{-1}^{1} dx\, \frac{t}{u-M_C^2} P_\ell(x) = (-1)^{\ell+1}\left\{\left(\frac{\langle t\rangle}{\Delta u} - z_C\right) Q_\ell(z_C) + \delta_{\ell 0}\right\} \tag{B.5}$$

$$h^{(\ell)}_{-.0} = \int_{-1}^{1} dx\, \frac{x}{u-M_C^2} P_\ell(x) = \frac{(-1)^\ell}{\Delta u}(z_C Q_\ell(z_C) - \delta_{\ell 0}) \tag{B.6}$$

$$h^{(\ell)}_{-.1} = \int_{-1}^{1} dx\, \frac{xu}{u-M_C^2} P_\ell(x) = (-1)^{\ell}\left\{z_C\left(z_C + \frac{\langle u\rangle}{\Delta u}\right) Q_\ell(z_C) - \left(z_C + \frac{\langle u\rangle}{\Delta u}\right)\delta_{\ell 0} - \frac{1}{3}\delta_{\ell 1}\right\} \tag{B.7}$$

$$\begin{aligned} h^{(\ell)}_{-.2} = \int_{-1}^{1} dx\, \frac{xu^2}{u-M_C^2} P_\ell(x) &= (-1)^{\ell}\left\{\frac{z_C}{\Delta u}\left(\langle u\rangle + z_C\Delta u\right)^2 Q_\ell(z_C)\right. \\ &\left. -\frac{1}{\Delta u}\left((\langle u\rangle + z_C\Delta u)^2 + \frac{1}{3}\Delta u^2\right)\delta_{\ell 0} - \frac{1}{3}(2\langle u\rangle + z_C\Delta u)\delta_{\ell 1} - \frac{2}{15}\Delta u\,\delta_{\ell 2}\right\} \end{aligned} \tag{B.8}$$

$$h^{(\ell)}_{-.3} = \int_{-1}^{1} dx\, \frac{xt}{u-M_C^2} P_\ell(x) = (-1)^{\ell+1}\left\{z_C\left(z_C - \frac{\langle t\rangle}{\Delta u}\right) Q_\ell(z_C) - \left(z_C - \frac{\langle t\rangle}{\Delta u}\right)\delta_{\ell 0} - \frac{1}{3}\delta_{\ell 1}\right\} \tag{B.9}$$

$$k^{(\ell)}_{-.0} = \int_{-1}^{1} dx\, \frac{1-x^2}{u-M_C^2} P'_\ell(x) = \frac{(-1)^{\ell+1}}{\Delta u}\frac{\ell(\ell+1)}{2\ell+1}(Q_{\ell+1}(z_C) - Q_{\ell-1}(z_C)) \tag{B.10}$$

$$k^{(\ell)}_{-.1} = \int_{-1}^{1} dx\, \frac{(1-x^2)u}{u-M_C^2} P'_\ell(x) = (-1)^{\ell+1}\frac{\ell(\ell+1)}{2\ell+1}\left\{\left(z_C + \frac{\langle u\rangle}{\Delta u}\right)(Q_{\ell+1}(z_C) - Q_{\ell-1}(z_C)) + \delta_{\ell 1}\right\} \tag{B.11}$$

$$\begin{aligned} k^{(\ell)}_{-.2} = \int_{-1}^{1} dx\, \frac{(1-x^2)u^2}{u-M_C^2} P'_\ell(x) &= (-1)^{\ell+1}\frac{\ell(\ell+1)}{2\ell+1}\left\{\frac{1}{\Delta u}(\langle u\rangle + z_C\Delta u)^2(Q_{\ell+1}(z_C) - Q_{\ell-1}(z_C))\right. \\ &\left. -\frac{\Delta u}{3}\delta_{\ell 0} + (2\langle u\rangle + z_C\Delta u)\delta_{\ell 1} + \frac{\Delta u}{3}\delta_{\ell 2}\right\} \end{aligned} \tag{B.12}$$

$$k^{(\ell)}_{-.3} = \int_{-1}^{1} dx\, \frac{(1-x^2)t}{u-M_C^2} P'_\ell(x) = (-1)^{\ell+1}\frac{\ell(\ell+1)}{2\ell+1}\left\{\left(-z_C + \frac{\langle t\rangle}{\Delta u}\right)(Q_{\ell+1}(z_C) - Q_{\ell-1}(z_C)) - \delta_{\ell 1}\right\} \tag{B.13}$$

For the vector-meson exchange partial waves in (21) we define,

$$y_c = \frac{{M_V}_c^2 - \langle t\rangle}{\Delta t}\ , \qquad c = 1, \ldots, 8\ . \tag{B.14}$$

Then, the integrals in (21b) can be obtained from the ones above with the substitutions.

$$\widetilde{h}^{(\ell)}_{\pm.i} = \left[h^{(\ell)}_{\pm.i}\right]^{\langle u\rangle\to\langle t\rangle}_{\substack{\Delta u\to -\Delta t\\ z_C\to -y_c}}\ , \qquad \widetilde{k}^{(\ell)}_{\pm.i} = \left[k^{(\ell)}_{\pm.i}\right]^{\langle u\rangle\to\langle t\rangle}_{\substack{\Delta u\to -\Delta t\\ z_C\to -y_c}}\ . \tag{B.15}$$

Notice that $Q_\ell(-z) = (-1)^{\ell+1}Q_\ell(z)$.

C Physics observables

In this appendix we summarize the expressions in terms of partial waves of the physics observables considered in sect. 4. The amplitude for the process $|B^a(p,\sigma)M^b(q)\rangle \longrightarrow |B^{a'}(p',\sigma')M^{b'}(q')\rangle$ is parameterized as,

$$\mathcal{T}^{ab}{}_{a'b'} \equiv \langle B_{a'}(p',\sigma')M_{b'}(q')|T|B^a(p,\sigma)M^b(q)\rangle = \overline{u}'(\Gamma_0{}^{ab}{}_{a'b'} + \Gamma_1{}^{ab}{}_{a'b'}\not{p}_T)u\ . \tag{C.1}$$

The associated partial-wave expansion is given in (2). Below, we omit flavor indices for simplicity. The total and differential cross sections are given in terms of partial waves by,

$$\sigma = \frac{(\hbar c)^2}{32\pi s}\frac{\omega(s,m_{a'}^2,\widetilde{m}_{b'}^2)}{\omega(s,m_a^2,\widetilde{m}_b^2)}\sum_{\ell=0}^{\infty}\frac{2}{2\ell+1}\left(|(\ell+1)f_{\ell+} + \ell f_{\ell-}|^2 + \ell(\ell+1)|f_{\ell+} - f_{\ell-}|^2\right), \tag{C.2}$$

$$\frac{d\sigma}{d\Omega} = \frac{(\hbar c)^2}{64\pi^2 s}\frac{\omega(s,m_{a'}^2,\widetilde{m}_{b'}^2)}{\omega(s,m_a^2,\widetilde{m}_b^2)}\left(\left|\sum_{\ell=0}^{\infty}\left((\ell+1)f_{\ell+}+\ell f_{\ell-}\right)P_\ell(x)\right|^2+(1-x^2)\left|\sum_{\ell=0}^{\infty}\left(f_{\ell+}-f_{\ell-}\right)P_\ell(x)\right|^2\right), \quad \text{(C.3)}$$

with the function ω defined in (A.1) and $x=\widehat{p}'\cdot\widehat{p}$ in the CMF.

If we denote $\mathcal{P}'$ the polarization of the final baryon in the CMF, the CMF spin asymmetry is given by [41],

$$\begin{aligned}\mathcal{A}' \equiv \frac{d\sigma}{d\Omega}\mathcal{P}' &= \frac{(\hbar c)^2}{64\pi^2 s}\frac{\omega(s,m_{a'}^2,\widetilde{m}_{b'}^2)}{\omega(s,m_a^2,\widetilde{m}_b^2)}\mathrm{Im}(\Gamma_0^*\Gamma_1)\left(-i\mathrm{Tr}\left(\not{p}\not{p}_T\not{p}'\ \not{s}'\gamma_5\right)\right)\ ,\\ &= \frac{(\hbar c)^2}{64\pi^2 s^{3/2}}\omega(s,m_{a'}^2,\widetilde{m}_{b'}^2)^2\sqrt{1-x^2}\mathrm{Im}(\Gamma_0^*\Gamma_1)\ ,\end{aligned} \quad \text{(C.4)}$$

where on the second line we set $s'^\mu=(0,\widehat{s}')$ with $\widehat{s}'=(\widehat{p}\wedge\widehat{p}')/|\widehat{p}\wedge\widehat{p}'|$, since we are interested in polarization orthogonal to the reaction plane, and used the definition of CM frame. Expanding in partial waves up to $\ell=2$ we obtain,

$$\begin{aligned}\mathcal{A}' = \frac{(\hbar c)^2}{32\pi^2 s}\frac{\omega(s,m_{a'}^2,\widetilde{m}_{b'}^2)}{\omega(s,m_a^2,\widetilde{m}_b^2)}\sqrt{1-x^2}\,\big\{&\mathrm{Im}\left((f_{1+}^*-f_{1-}^*)f_0\right)+\mathrm{Im}\left((f_{1+}^*-f_{1-}^*)(3f_{2+}+2f_{2-})\right)P_2(x)\\ &+\mathrm{Im}\left((f_{2+}^*-f_{2-}^*)f_0\right)P_2'(x)+\mathrm{Im}\left((f_{2+}^*-f_{2-}^*)(2f_{1+}+f_{1-})\right)P_2'(x)P_1(x)+3\mathrm{Im}\left(f_{1+}^*f_{1-}\right)P_1(x)\\ &+5\mathrm{Im}\left(f_{2+}^*f_{2-}\right)P_2'(x)P_2(x)\big\}\ .\end{aligned} \quad \text{(C.5)}$$

The Legendre moments of the differential cross section and spin asymmetry are defined as [55, 57],

$$\frac{d\sigma}{d\Omega}=\sum_{n=0}^{\infty}A_nP_n(x)\ ,\qquad \frac{d\sigma}{d\Omega}\mathcal{P}'=\sqrt{1-x^2}\sum_{n=1}^{\infty}B_nP_n'(x)\ . \quad \text{(C.6)}$$

The moments A_n, B_n can be expressed in terms of partial waves. For notational convenience we define,

$$a_0\equiv|f_0|^2+\frac{1}{3}|2f_{1+}+f_{1-}|^2+\frac{1}{5}|3f_{2+}+2f_{2-}|^2+\frac{2}{3}|f_{1+}-f_{1-}|^2+\frac{6}{5}|f_{2+}-f_{2-}|^2\ . \quad \text{(C.7)}$$

We thus have the partial-wave expansions, up to D wave,

$$\begin{aligned}A_0 &= \frac{\sigma}{4\pi}=\frac{(\hbar c)^2}{32\pi s}\frac{\omega(s,m_{a'}^2,\widetilde{m}_{b'}^2)}{\omega(s,m_a^2,\widetilde{m}_b^2)}a_0\ ,\\ a_0\frac{A_1}{A_0} &= 2\mathrm{Re}\left(f_0(2f_{1+}^*+f_{1-}^*)\right)+\frac{4}{5}\mathrm{Re}\left((2f_{1+}+f_{1-})(3f_{2+}^*+2f_{2-}^*)\right)\\ &\quad+\frac{12}{5}\mathrm{Re}\left((f_{1+}-f_{1-})(f_{2+}^*-f_{2-}^*)\right),\\ a_0\frac{A_2}{A_0} &= 2\mathrm{Re}\left(f_0(3f_{2+}^*+2f_{2-}^*)\right)+\frac{2}{3}\left|2f_{1+}+f_{1-}\right|^2+\frac{2}{7}\left|3f_{2+}+2f_{2-}\right|^2-\frac{2}{3}\left|f_{1+}-f_{1-}\right|^2\\ &\quad+\frac{6}{7}\left|f_{2+}-f_{2-}\right|^2\ ,\\ a_0\frac{B_1}{A_0} &= 2\mathrm{Im}\left((f_{1+}^*-f_{1-}^*)f_0\right)-\frac{2}{5}\mathrm{Im}\left((f_{1+}^*-f_{1-}^*)(3f_{2+}+2f_{2-})\right)\\ &\quad+\frac{6}{5}\mathrm{Im}\left((f_{2+}^*-f_{2-}^*)(2f_{1+}+f_{1-})\right)\ ,\\ a_0\frac{B_2}{A_0} &= 2\mathrm{Im}\left(f_{1+}^*f_{1-}\right)+2\mathrm{Im}\left((f_{2+}^*-f_{2-}^*)f_0\right)+\frac{10}{7}\mathrm{Im}\left(f_{2+}^*f_{2-}\right)\ .\end{aligned} \quad \text{(C.8)}$$

The threshold branching fractions are defined as [51, 52],

$$\gamma=\left.\frac{\sigma_{pK^-\to\Sigma^-\pi^+}}{\sigma_{pK^-\to\Sigma^+\pi^-}}\right|_{\rm thr}\ ,\quad R_c=\left.\frac{\sigma_{pK^-\to\rm charged}}{\sigma_{pK^-\to\rm all}}\right|_{\rm thr}\ ,\quad R_n=\left.\frac{\sigma_{pK^-\to\Lambda\pi^0}}{\sigma_{pK^-\to\rm all\ neutral}}\right|_{\rm thr}\ . \quad \text{(C.9)}$$

Finally, with our normalization the scattering length is expressed as,

$$a_{pK^-}=\frac{\hbar c}{4\pi}\frac{1}{2m_p}\frac{1}{1+m_{K^-}/m_p}\left(f_0^{45\ 45}\right)_{\rm thr}\ , \quad \text{(C.10)}$$

with $(f_0^{45\ 45})_{\rm thr}$ the S wave for elastic pK^- scattering evaluated at threshold. Thus, $(\sigma)_{\rm thr}=4\pi|a_{pK^-}|^2$.

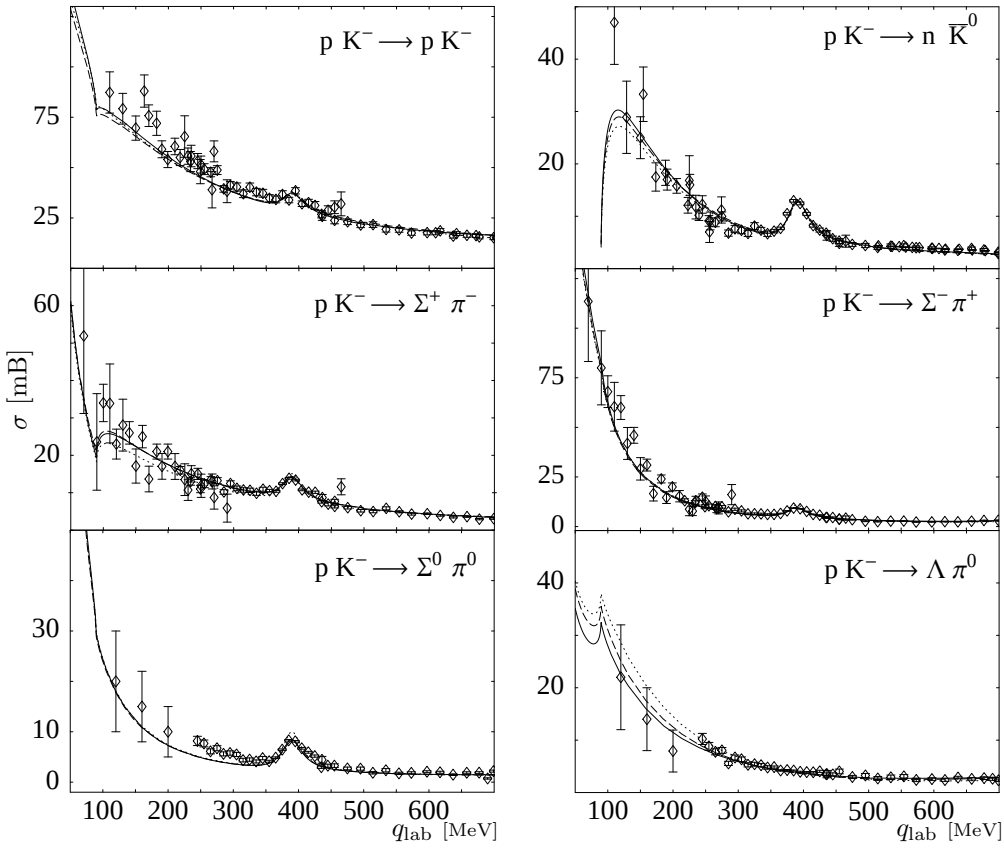

Figure 1: Total cross sections for pK^- scattering. Solid lines: fit I, which includes all amplitudes described in sect. 2. Dashed lines: fit II, which includes only $\mathcal{O}(q^1)$ amplitudes. Dotted lines: fit III, which includes $\mathcal{O}(q^1)$ amplitudes except vector-meson exchange ones. Data from [53–61].

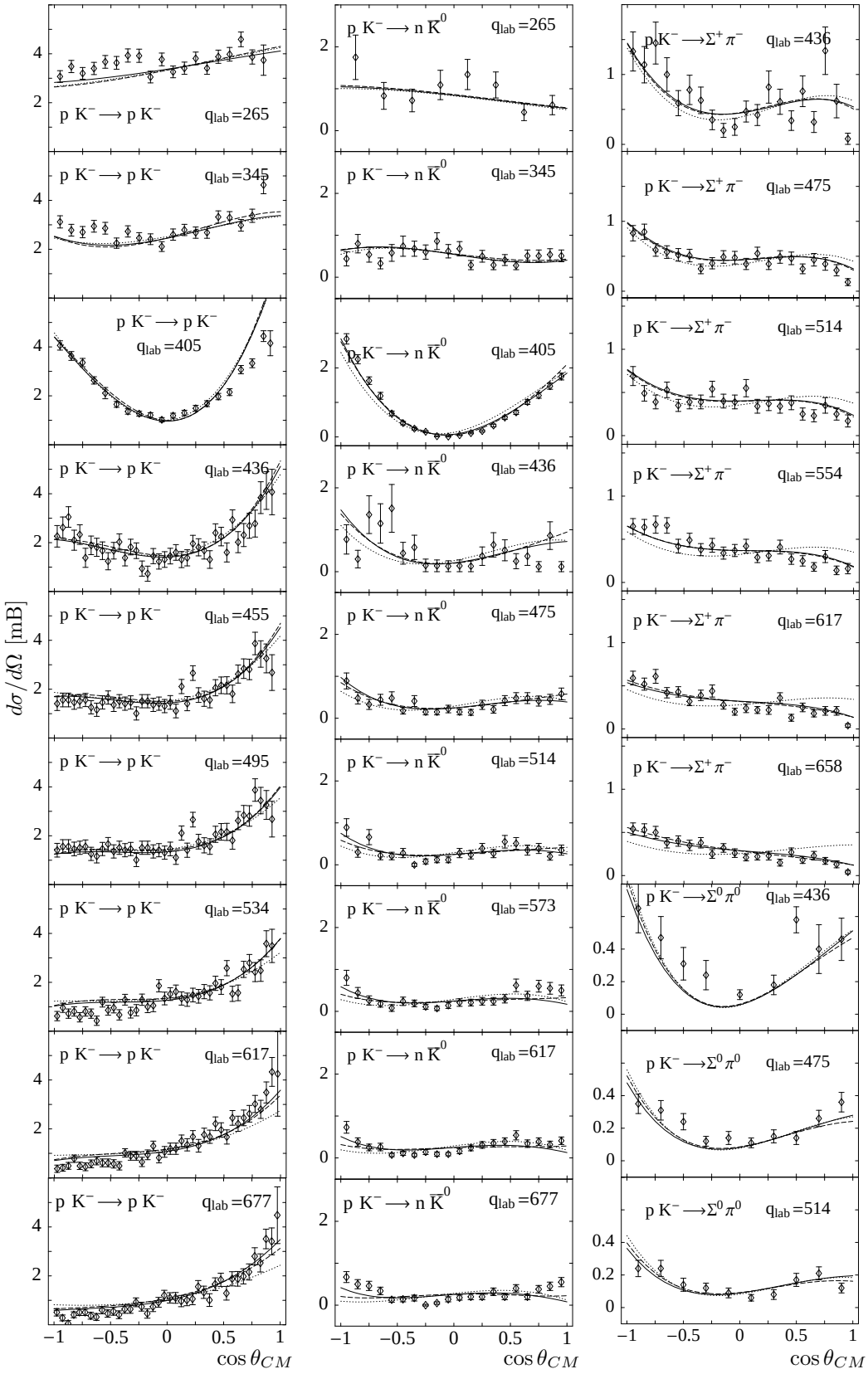

Figure 2: Differential cross sections for pK^- scattering. Solid, dashed and dotted lines as in fig. 1. Only a representative sample of data from [54, 56] is shown.

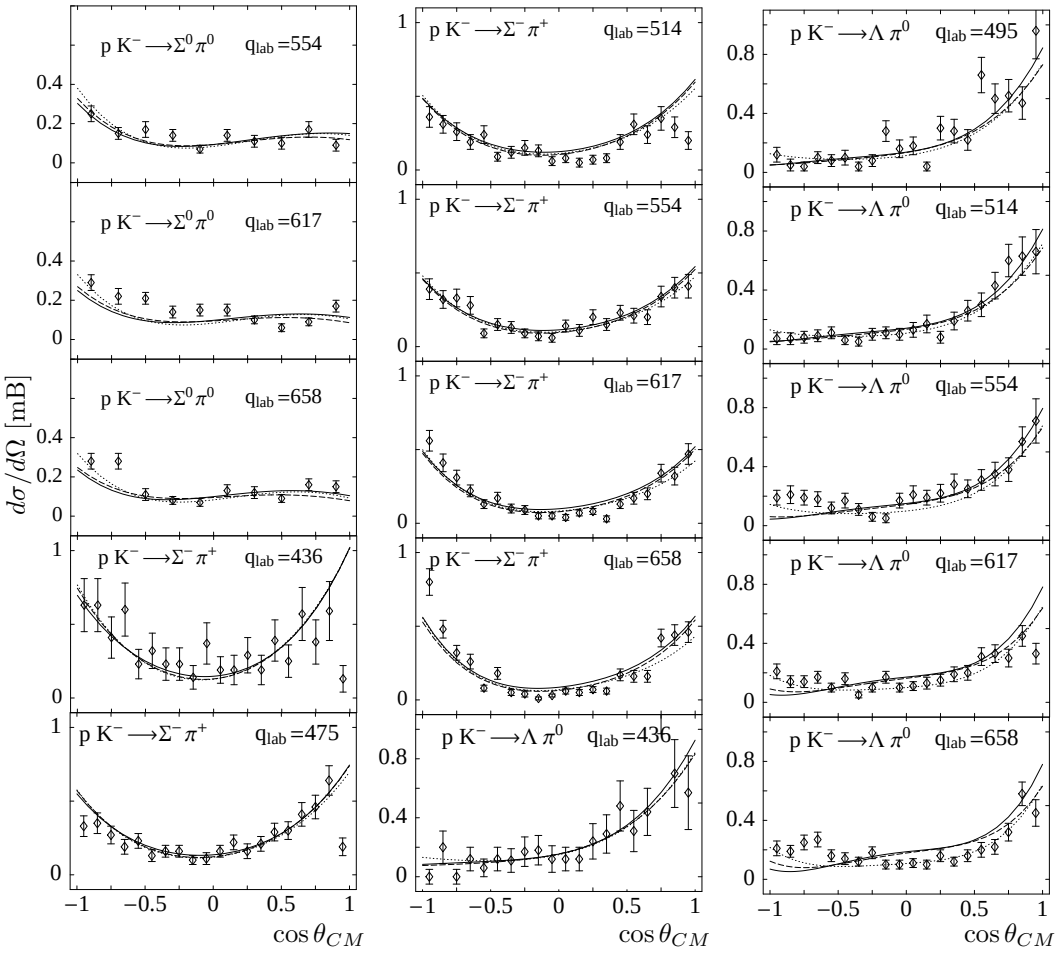

Figure 2: Continued.

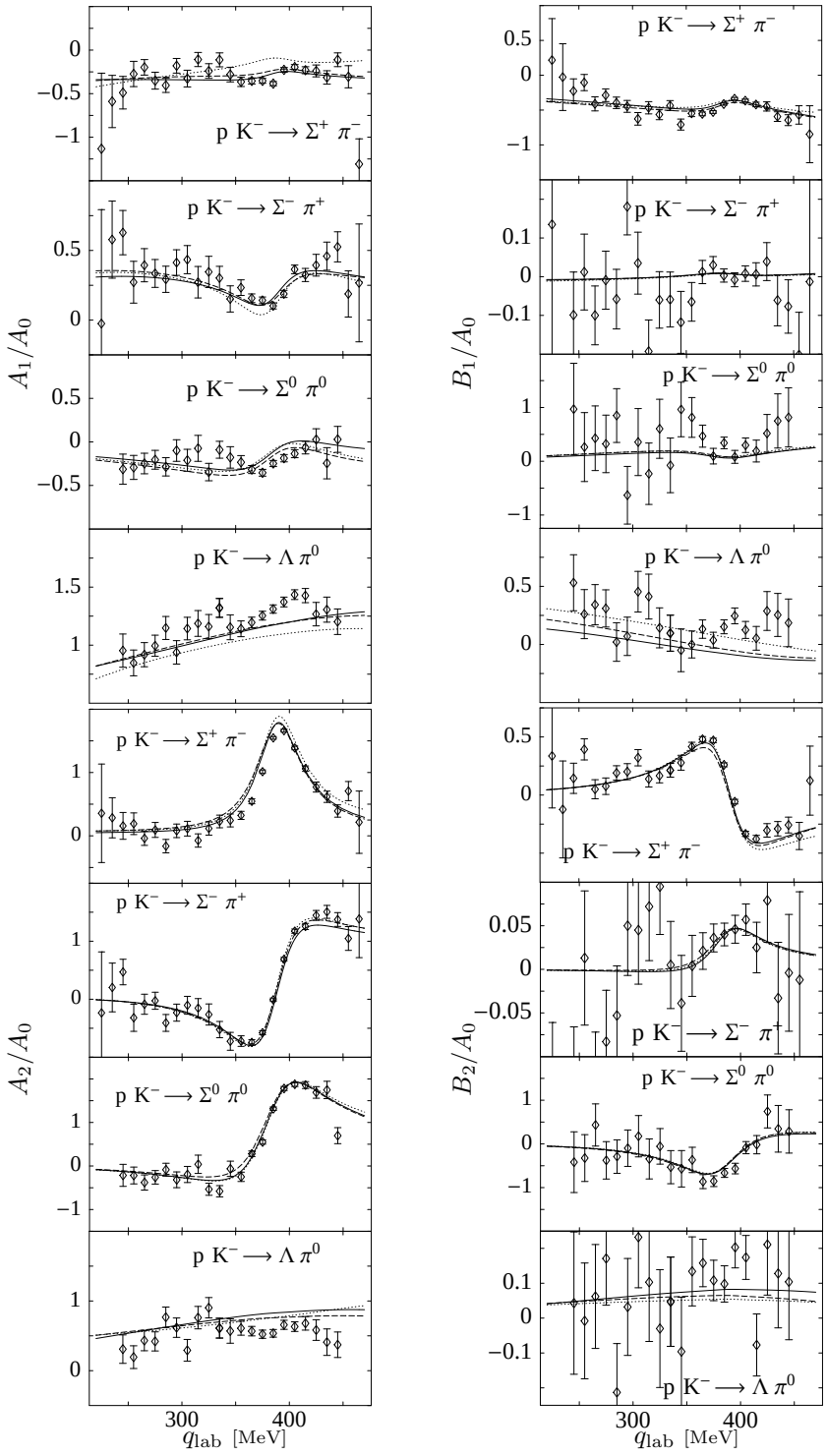

Figure 3: Legendre moments of differential cross sections and spin asymmetries for pK^- scattering. Solid, dashed and dotted lines as in fig. 1. Data from [55, 57, 58].

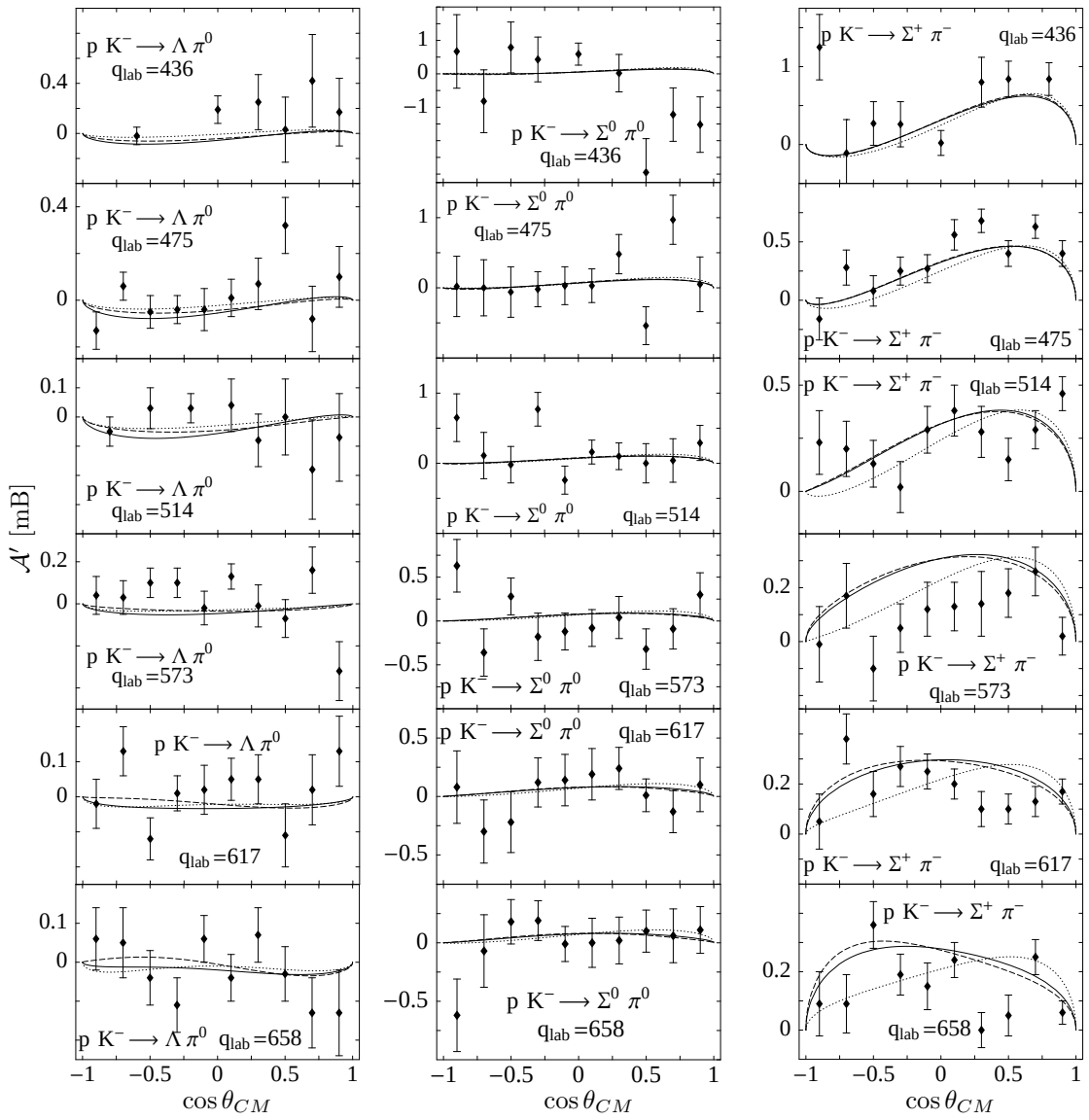

Figure 4: Center-of-mass frame spin asymmetry for pK^- scattering. Solid, dashed and dotted lines as in fig. 1. Data from [54].

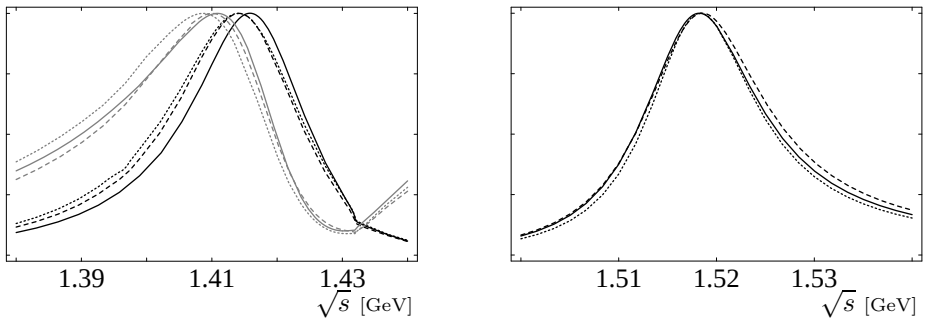

Figure 5: $\Sigma\pi$ mass spectrum for isosinglet partial waves, in arbitrary units. Left panel: $S_{1/2}$ wave, $\Sigma\pi \to \Sigma\pi$ (gray lines) and $NK \to \Sigma\pi$ (black lines). Right panel: $D_{3/2}$ wave, $NK \to \Sigma\pi$. Solid, dashed and dotted lines as in fig. 1.